

Impact splash chondrule formation during planetesimal recycling

Tim Lichtenberg^{a,b,*}, Gregor J. Golabek^c, Cornelis P. Dullemond^d, Maria Schönbachler^e, Taras V. Gerya^a, Michael R. Meyer^{b,f}

^a*Institute of Geophysics, ETH Zürich, Sonneggstrasse 5, 8092 Zürich, Switzerland*

^b*Institute for Astronomy, ETH Zürich, Wolfgang-Pauli-Strasse 27, 8093 Zürich, Switzerland*

^c*Bayerisches Geoinstitut, University of Bayreuth, Universitätsstrasse 30, 95440 Bayreuth, Germany*

^d*Institute for Theoretical Astrophysics, Zentrum für Astronomie, Heidelberg University, Albert-Ueberle-Strasse 2, 69120 Heidelberg, Germany*

^e*Institute of Geochemistry and Petrology, ETH Zürich, Clausiusstrasse 25, 8092 Zürich, Switzerland*

^f*Department of Astronomy, University of Michigan, 1085 S. University Avenue, Ann Arbor, MI 48109, USA*

Abstract

Chondrules, mm-sized igneous-textured spherules, are the dominant bulk silicate constituent of chondritic meteorites and originate from highly energetic, local processes during the first million years after the birth of the Sun. So far, an astrophysically consistent chondrule formation scenario explaining major chemical, isotopic and textural features, in particular Fe, Ni metal abundances, bulk Fe/Mg ratios and intra-chondrite chemical and isotopic diversity, remains elusive. Here, we examine the prospect of forming chondrules from impact splashes among planetesimals heated by radioactive decay of short-lived radionuclides using thermomechanical models of their interior evolution. We show that intensely melted planetesimals with interior magma oceans became rapidly chemically equilibrated and physically differentiated. Therefore, collisional interactions among such bodies would have resulted in chondrule-like but basaltic spherules, which are not observed in the meteoritic record. This inconsistency with the expected dynamical interactions hints at an incomplete understanding of the planetary growth regime during the lifetime of the solar protoplanetary disk. To resolve this conundrum, we examine how the observed chemical and isotopic features of chondrules constrain the dynamical environment of accreting chondrite parent bodies by interpreting the meteoritic record as an impact-generated proxy of early solar system planetesimals that underwent repeated collision and reaccretion cycles. Using a coupled evolution-collision model we demonstrate that the vast majority of collisional debris feeding the asteroid main belt must be derived from planetesimals which were partially molten at maximum. Therefore, the precursors of chondrite parent bodies either formed primarily small, from sub-canonical aluminum-26 reservoirs, or collisional destruction mechanisms were efficient enough to shatter planetesimals before they reached the magma ocean phase. Finally, we outline the window in parameter space for which chondrule formation from planetesimal collisions can be reconciled with the meteoritic record and how our results can be used to further constrain early solar system dynamics.

Keywords:

Chondrule formation, Meteorites, Planetary formation, Planetesimals, Thermal histories

1. Introduction

Chondrules are igneous-textured spherules, typically 0.1–2 mm in diameter, and largely composed of the silicate minerals olivine and pyroxene. They are abundantly found in chondritic meteorites, together with other disk materials, such as Ca, Al-rich inclusions (CAIs) and the fine-grained matrix that includes presolar grains and primitive organics (Scott and Krot, 2014). Chondrules are often surrounded by or close to beads of Fe, Ni metal (e.g., Wasson and Rubin, 2010; Jones, 2012) and show specific features, such as high abundances of moderately volatile elements like Na, K and S (Alexander et al., 2008; Scott and Krot, 2014; Connolly and Jones, 2016) and diverse chemical and isotopic signatures (Jones and Schilk, 2009; Hezel and Palme, 2010; Olsen et al., 2016). Their peak temperatures were ~ 1900 K or higher (Alexander et al., 2008; Connolly and Jones, 2016)

with subsequent cooling in minutes to days (e.g., Hewins et al., 2012; Desch et al., 2012; Wick and Jones, 2012). Most chondrules were formed during the earliest phases of the solar system within the first 3–4 million years after the formation of CAIs (e.g., Villeneuve et al., 2009; Connelly et al., 2012) and show clear evidence for multiple melting cycles (Rubin, 2017, and references therein).

Because of their enigmatic features coupled with high-energy processing, chondrule formation is considered to be intimately linked to the physical processes in the protoplanetary disk or planetary accretion and spawned a multitude of proposed formation mechanisms. The often underlying view of how chondrules are intertwined with the planet formation process is that they were formed before accretion and therefore represent the fundamental building materials of the planets and asteroids (Connolly and Jones, 2016). In this case, chondrules are formed before parent body accretion, either by melting dust aggregates by nebular shocks (Desch and Connolly, 2002; Morris and Desch, 2010; Morris et al.,

*Corresponding author. E-mail: tim.lichtenberg@phys.ethz.ch.

2016), for example related to global disk instabilities (Boss and Durisen, 2005; Lichtenberg and Schleicher, 2015), or condensation of melts and crystals (Blander et al., 2004; Nagahara et al., 2008). In contrast, if chondrules formed via processes involving already formed planetesimals, the interpretation of their role would shift to a ‘by-product’ of planet(esimal) formation (see discussion in Section 4).

Recently proposed chondrule formation scenarios considered melt spray from subsonic collisions (‘splashes’) between similar-sized planetesimals, which were fully melted by decay heat from ^{26}Al (Asphaug et al., 2011; Sanders and Scott, 2012) or impact ‘jetting’ via collisions of planetesimals with undifferentiated protoplanets (Johnson et al., 2015; Hasegawa et al., 2016; Wakita et al., 2017). Collisional mechanisms were suggested previously and offer attractive solutions to many chondrule features (Krot et al., 2005; Sanders and Scott, 2012; Stammer and Dullemond, 2014; Dullemond et al., 2014, 2016; Marrocchi et al., 2016). From a dynamical point-of-view, collisional interactions of planetesimals and embryos during accretion are inevitable and expected to create a vast amount of continuously reprocessed debris (Bottke et al., 2006; Carter et al., 2015; Jacobson and Walsh, 2015; Asphaug, 2017; Bottke and Morbidelli, 2017) that inherits the geochemical features from previous planetesimal generations.

Collisional models of chondrule formation considering fully-molten planetesimals, and thus highly energetic internal magma oceans with temperatures above the liquidus (Asphaug et al., 2011; Sanders and Scott, 2012), have the advantage that bodies interacting at low speeds (\sim around the two-body escape velocity) can cause a melt spray ejection into the ambient disk medium that provides the inferred cooling regime for chondrules and the required solid densities to preserve primitive abundances of moderately volatile elements (Sanders and Scott, 2012; Dullemond et al., 2014, 2016).

For consistency with the observed metal abundances in and around chondrules (Wasson and Rubin, 2010; Palme et al., 2014; Connolly and Jones, 2016), droplet entrainment in a vigorously convecting magma ocean has been invoked to prevent efficient and complete metal-silicate segregation (Asphaug et al., 2011; Sanders and Scott, 2012; Asphaug, 2017). However, metal sequestration into the planetesimal core may have been rapid in magma ocean planetesimals as, for instance, supported by the old ages of iron meteorites (Kruijjer et al., 2014). In this case, re-establishing post-collisional bulk Fe/Mg ratios and forming chondrites with metal beads would require a complicated and highly unlikely scenario of (i) partial oxidization of the metal cores of fully differentiated planetesimals and (ii) violent remixing of the remaining metal core material with mantle silicates during or after the collision (Palme et al., 2015). Additionally, chemical (Jones et al., 2005; Hezel and Palme, 2007; Palme et al., 2014) and isotopic (Bauer et al., 2016; Olsen et al., 2016) heterogeneities between single chondrules of the same meteorite cannot be retained if vigorous convection at low silicate viscosities homogenized the bulk volume of primitive

planetesimals down to chondrule-sized microscales.

However, it is well known that the interior evolution of planetesimals alone could create a diverse range of thermal histories and interior structures (e.g., Hevey and Sanders, 2006; Lichtenberg et al., 2016a), where magma ocean planetesimals are only one end-member type. In addition, the structure and chemistry of planetary materials was potentially further altered due to repeated collision–reaccretion cycles, which may generate varying thermal and chemical histories on a cm–m scale of planetary materials. Here, we probe the thermal and chemical evolution of such debris in a dynamical setting for the early solar system, where small (< 100 km) planetesimals were continuously formed over a given time-frame during the lifetime of the circumstellar disk, evolved internally due to radiogenic heating, and were subsequently destroyed by collisions. To evaluate the thermal and chemical state of the debris over time, we quantify the processes governing metal-silicate segregation and chemical diversity within molten planetesimals and model their thermal histories dependent on their sizes and initial ^{26}Al abundances. To classify the parameter space that is (in-)consistent with chondrule formation from impact splashes among similar-sized planetesimals, we calculate the combined influence of interior evolution and collisional parameters in a simple Monte Carlo model. We describe our methodology in Section 2 and show the results from our scalings and computations in Section 3. We discuss our findings and the limits of our approach in Section 4, and draw conclusions in Section 5.

2. Methods

2.1. Scaling analysis

This first part of our analysis aims to quantify the thermochemical processes governing the interior of planetesimals with high melt fractions above the rheological transition. The rheological transition of silicates describes the critical melt fraction $\varphi_{\text{crit}} \sim 0.4\text{--}0.6$ (Costa et al., 2009) at which the silicate viscosity drops by orders of magnitude (from rock- to water-like behavior). At this range, the dynamic state of the system changes from solid-state creep processes to liquid-like convectational motions in an interior magma ocean. Here, we describe the processes in an idealized system that represents the end-member scenario of a planetesimal that has fully melted as a result of ^{26}Al decay.

2.1.1. Metal-silicate segregation from Fe,Ni droplet rainfall

For the case of a fully-molten planetesimal, we parameterize the rain-out of Fe,Ni metal droplets following the description by Solomatov (2015). The dynamic processes in the magma ocean are determined by its viscosity, which drops by orders of magnitude at the rheological transition $\varphi_{\text{crit}} \sim 0.4\text{--}0.6$ (Costa et al., 2009), from $\eta \sim 10^{17}$ Pa s to 10^{-2} Pa s (Rubie et al., 2003; Liebske et al., 2005), as listed in Table 1. In melt regimes valid for planetesimals, the convective heat

Table 1: List of physical parameters used.

PARAMETER	SYMBOL	VALUE	UNIT	REFERENCES
Density of uncompressed solid silicates	$\rho_{\text{Si-sol}}$	3500	kg m ⁻³	(1,2)
Density of uncompressed molten silicates	$\rho_{\text{Si-liq}}$	2900	kg m ⁻³	(1)
Density of uncompressed iron	ρ_{Fe}	7540	kg m ⁻³	(3)
Ambient temperature	T_0	290	K	(3,4)
Activation energy	E_a	470	kJ mol ⁻¹	(5)
Dislocation creep onset stress	σ_0	$3 \cdot 10^7$	Pa	(6)
Power law exponent	n	4	non-dim.	(5)
Latent heat of silicate melting	L_{Si}	400	kJ kg ⁻¹	(3,6)
Melt fraction at rheological transition	φ_{crit}	0.4	non-dim.	(8,9)
Silicate heat capacity	c_p	1000	J kg ⁻¹ K ⁻¹	(6)
Thermal diffusivity	κ	$1 \cdot 10^{-6}$	m ² s ⁻¹	(6)
Thermal expansivity of solid silicates	$\alpha_{\text{Si-sol}}$	$3 \cdot 10^{-5}$	K ⁻¹	(2)
Thermal expansivity of molten silicates	$\alpha_{\text{Si-liq}}$	$6 \cdot 10^{-5}$	K ⁻¹	(2)
Thermal expansivity of iron	α_{Fe}	$1 \cdot 10^{-5}$	K ⁻¹	(9)
Thermal conductivity of solid silicates	k	3	W m ⁻¹ K ⁻¹	(10)
Thermal conductivity of molten silicates	k_{eff}	$\leq 10^6$	W m ⁻¹ K ⁻¹	(11)
Min. unsintered silicate thermal conductivity	k_{low}	10^{-3}	W m ⁻¹ K ⁻¹	(12,13)
Temperature at onset of hot sintering	T_{sint}	700	K	(12)
Peridotite solidus temperature	T_{sol}	1416	K	(14)
Peridotite liquidus temperature	T_{liq}	1973	K	(15)
Lower cut-off viscosity	η_{num}	10^{17}	Pa s	(16)
Silicate melt viscosity	η_{melt}	10^{-2}	Pa s	(17)
Droplet surface energy	σ	1	N m ⁻¹	(18)
Chemical diffusivity of silicates	κ_C	10^{-8}	m ² s ⁻¹	(18)

References: (1) Stolper et al. (1981), (2) Suzuki et al. (1998), (3) Ghosh and McSween (1998), (4) Barshay and Lewis (1976), (5) Ranalli (1995), (6) Turcotte and Schubert (2014), (7) Costa et al. (2009), (8) Solomatov (2015), (9) Boehler et al. (1990), (10) Tarduno et al. (2012), (11) Golabek et al. (2014), (12) Yomogida and Matsui (1984), (13) Henke et al. (2012), (14) Herzberg et al. (2000), (15) Trønnes and Frost (2002), (16) Lichtenberg et al. (2016a), (17) Liebske et al. (2005), (18) Rubie et al. (2003)

flux q of the magma ocean can be calculated via

$$q = 0.089k \frac{(T_m - T_0)Ra^{1/3}}{D}, \quad (1)$$

with Rayleigh number

$$Ra = \alpha_{\text{Si-liq}} g \rho_{\text{ref}} \frac{(T_m - T_0)D^3}{\kappa \eta}, \quad (2)$$

potential temperature T_m , ambient (and surface) temperature $T_0 = 290$ K, thermal diffusivity $\kappa = k/(\rho c_p)$, thermal conductivity of solid silicates k , silicate heat capacity c_p , thermal expansivity of molten silicates $\alpha_{\text{Si-liq}}$, depth of the magma ocean D , silicate densities

$$\rho_s = \rho_{\text{sol}} - (\rho_{\text{sol}} - \rho_{\text{liq}}) \cdot \varphi, \quad (3)$$

$$\rho_{\text{sol}} = \rho_{\text{Si-sol}} \cdot (1 - \alpha_{\text{Si-sol}} \cdot [T - T_0]), \quad (4)$$

$$\rho_{\text{liq}} = \rho_{\text{Si-liq}} \cdot (1 - \alpha_{\text{Si-liq}} \cdot [T - T_0]), \quad (5)$$

temperature T and thermal expansivity of solid silicates $\alpha_{\text{Si-sol}}$. See Table 1 for the numerical values used. The convective velocities are then

$$v_s \approx 0.6 \left(\frac{\alpha_{\text{Si-liq}} g l q}{\rho_s c_p} \right)^{1/3}, \quad (6)$$

with gravity g , and mixing length $l \sim D \sim R_p$. Based on laboratory experiments, it has been shown that droplets can

be suspended (or re-entrained) by the convective flow if their diameter is

$$d \leq \frac{\rho_s (v_s / x_*)^2}{0.1(\rho_m - \rho_s)g}, \quad (7)$$

with metal density

$$\rho_m = \rho_{\text{Fe}} \cdot (1 - \alpha_{\text{Fe}} \cdot [T - T_0]), \quad (8)$$

thermal expansivity of iron α_{Fe} and constant factor $x_* = 60$ (Solomatov, 2015). Metal droplets suspended in the magma tend to be drawn together into spherical droplets, minimizing their surface area. Their stability is determined by the ratio between the stagnation pressure and the internal pressure caused by surface tension, given by the Weber number We , which can be used to estimate the expected sizes of droplet diameters

$$d = \frac{\sigma \cdot We}{(\rho_m - \rho_s)v_s^2}, \quad (9)$$

with surface energy σ , where $We \leq 10$ is the stability threshold (Rubie et al., 2003). For a given depth of the magma ocean $D \sim R_p$, melt fraction φ , and the numerical values listed in Table 1, we can determine the ratio of the expected droplet sizes and the upper limits for suspension (Section 3.1, Figure 3). The expected droplet size must be smaller

than the upper limit for suspension for the droplets to be entrained in the flow and resist rain-out onto the planetesimal core.

2.1.2. Chemical equilibration via turbulent diffusion

Metal-silicate separation via the rainfall mechanism is not the only process that shapes the interior dynamics of a fully-molten planetesimal. Chemical and nucleosynthetic heterogeneities, inherited from the solar nebula prior to planetesimal formation, can be erased by large-scale convective mixing once the silicate rheology transitions to fluid-like behaviour. In addition to planetesimal-scale mixing, chemical diffusion (Rubie et al., 2003) from dissipation of turbulent energy down to the so-called Kolmogorov microscales affects chondrule- and grain-sized regions – the precursor material for chondrules in the splashing model. The time scale at which neighbouring cells achieve such microscale chemical equilibration can be estimated via the local diffusion time scale

$$t_{\text{eq}} = l_{\text{K}}^2 / \kappa_{\text{C}}, \quad (10)$$

with the Kolmogorov length scale l_{K} and the chemical diffusivity κ_{C} (Table 1). The Kolmogorov length scale is given as

$$l_{\text{K}} = \left(\frac{\eta_{\text{melt}}^3 D}{\rho_{\text{Si-liq}}^3 v_s^3} \right)^{1/4}, \quad (11)$$

with the viscosity of the magma ocean η_{melt} , the density of molten silicates $\rho_{\text{Si-liq}}$ and v_s the convection velocity in the magma ocean calculated from Equation 6. Like in the section before, we choose to approximate the magma ocean length scale D with the planetesimal radius R_{P} , because in turbulent systems the dissipation rate at the smallest scales is primarily determined by the length scale of total kinetic energy in the turbulent motions; that is, the planetesimal radius in the case of a fully-molten magma ocean planetesimal. Using these scalings, we compute the time scales for diffusion, dependent on the radius of the planetesimal and the silicate viscosity.

In addition, we plot the time scales for collisions between similar-sized objects (Asphaug, 2010) in a planetesimal collision setting using

$$t_{\text{coll}} = \frac{2R_{\text{P}}}{\Delta v} \quad (12)$$

with the impact velocity Δv . Using the parameters given in Table 1, we derive scalings for various melt fractions, planetesimal radii and impact velocities, which are displayed in Figure 4 (Section 3.1).

2.2. Thermomechanical evolution of planetesimals

To bring the former calculations into context, we now consider the time-dependent interior evolution of planetesimals participating in potential chondrule-forming collisions in the early solar system. To do so, we model their thermomechanical histories using two-dimensional fluid dynamics simulations employing a conservative finite-differences

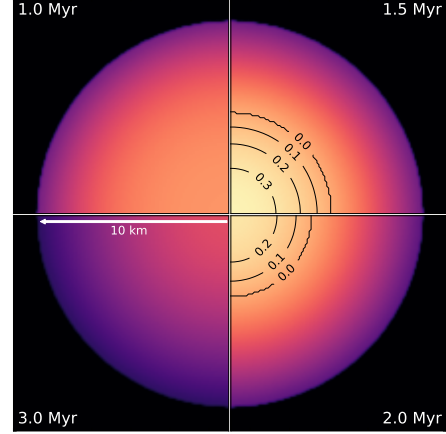


Figure 1: Thermal evolution of a planetesimal that is 10 km in radius and formed at 0.5 Myr after CAIs in our 2D cylinder geometry models. Silicate melt fractions are indicated with black isolines, and the temperature color scale ranges linearly from ~ 290 K (black) to ~ 1650 K (bright yellow).

fully-staggered grid formulation (Gerya and Yuen, 2003, 2007). The numerical model is described in detail in Golabek et al. (2014) and Lichtenberg et al. (2016a, and references therein), which is why we only briefly summarize its main characteristics here. The code solves the continuity, Stokes and location-dependent Poisson equation for self-gravity of material together with the energy equation, which includes source terms for radiogenic, shear and latent heat production. Physical properties are advanced using Lagrangian markers to minimize numerical diffusion and capture sharp viscosity and temperature gradients. To account for the solar system-specific ^{26}Al heating term (Lichtenberg et al., 2016b), the so-called ‘canonical’ abundance of $^{26}\text{Al}/^{27}\text{Al} = 5.25 \cdot 10^{-5}$ at CAI formation (Kita et al., 2013) is adopted.

The silicate melt is parameterized according to a peridotitic composition, taking into account both consumption and release of latent heat. For melt fractions $\varphi \geq 0.4$ the convective heat flux is approximated using the soft turbulence formulation (Kraichnan, 1962; Siggia, 1994). All our models incorporate an initial macroporosity (inverse filling-factor) of $\phi_{\text{init}} = 0.3$, where sintering and compaction effects are parameterized using constraints from laboratory experiments (Henke et al., 2012; Gail et al., 2015).

The numerical models were run using a two-dimensional infinite cylinder geometry on a Cartesian grid, starting from ambient temperature of $T_0 = 290$ K, as for such small bodies accretionary heat is insignificant (Schubert et al., 1986; Elkins-Tanton et al., 2011), and are surrounded by a low-density and low-viscosity layer of ‘sticky air’ that serves as heat sink (Schmeling et al., 2008; Crameri et al., 2012). The parameter space investigated spans the regime of $R_{\text{P}} = 10\text{--}100$ km in steps of 10 km, and $t_{\text{form}} = 0.1\text{--}1.5$ Myr after CAIs in steps of 0.1 Myr, the potential formation time interval of chondrule precursor material (Luu et al., 2015). Illustrations of the two-dimensional temperature and melt fraction evolution for a single simulation and the entire simulation grid are shown in Figure 1 and Figure 2, respectively. Further visual-

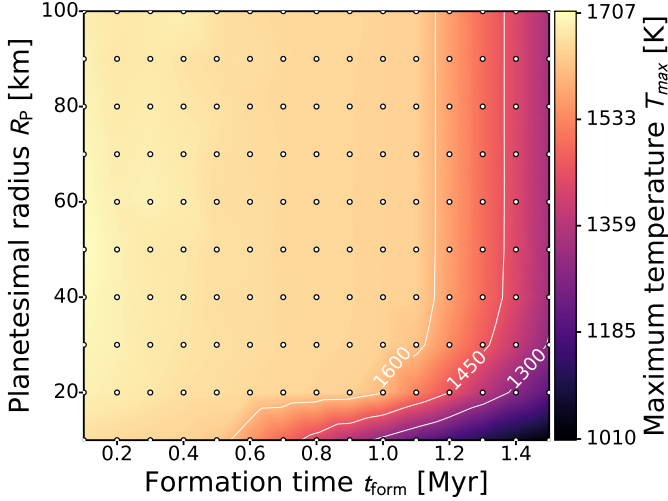


Figure 2: Maximum temperatures T_{\max} reached within planetesimals of radius R_p and formation time t_{form} . Small planetesimals below 20–30 km in radius reach significantly lower temperatures than larger bodies for a given formation time.

izations and analyses of the major qualitative regimes of the time-dependent thermal and density evolution are shown in Lichtenberg et al. (2016a).

Importantly, our model utilizes a scaling for the cooling of a low-viscosity magma ocean, in which the effective thermal conductivity across finite-difference nodes is given as

$$k_{\text{eff}} = (q/0.089)^{3/2} \cdot \frac{\alpha_{\text{Si-liq}} g c_p}{\Delta T^2 \rho_s \eta_{\text{num}}} \quad (13)$$

with the convective heat flux q , the temperature difference across the nodes ΔT , the silicate density ρ_s , the thermal expansivity $\alpha_{\text{Si-liq}}$, gravity g , and the lower cut-off viscosity $\eta_{\text{num}} = 10^{17}$ Pa s. This effective heat flux numerically approximates the increased heat flux during magma ocean stages and results in a more effective cooling of regions which are subject to the highest temperatures (Hevey and Sanders, 2006; Lichtenberg et al., 2016a). We use these interior evolution models to determine the time-dependent thermal structure of the planetesimals together with the scalings from Section 2.1.1 and 2.1.2 to evaluate which parts of their interior can be eligible as chondrule precursor bodies at a given time after the formation of CAIs.

2.3. Evolution-collision model

The evolution of the precursor bodies is important to understand the energetic state and evolution of the silicates before the chondrule forming impact event. However, if the planetesimal body is not *fully* molten ($\varphi < \varphi_{\text{crit}}$), the impact energy is necessary to elevate the silicate temperatures to above the chondrule formation temperature of $T_{\text{chondrule}} \geq 1900$ K and eject the molten material from the two bodies. When material is freed from the colliding bodies during the impact, it is first compressed by the impact shock wave and then decompressed after ejection. By this process, fractions

of the lithostatic/hydrostatic pressure within the planetesimal are converted into surface energy of magma (chondrule) droplets (Asphaug et al., 2011; Asphaug, 2017). In order to produce a melt spray that is consistent with the thermal histories of chondrules, at least parts of the material must have been heated to $T_{\text{chondrule}} \geq 1900$ K (Alexander et al., 2008; Connolly and Jones, 2016) and subsequently cool down in an emerging droplet cloud of high density (Dullemond et al., 2014, 2016).

In order to demonstrate the influence of the pre-collision state on chondrule thermal histories and the post-collision energy distribution, we have developed a Monte Carlo approach. The *a priori* assumption for this model is that planetesimals collide continuously during 0–5 Myr after CAI formation. Furthermore, when bodies collide, they generate debris and new planetesimals may be created from this material. For the moment, bodies from primordial and reaccreted material are treated the same, i.e., the material does not have a chemical ‘memory’ of prior generations. We discuss these and other assumptions in Section 4.

We start by randomly generating planetesimals in agreement with a radius power law

$$dN/dR_p \propto R_p^{-q}, \quad (14)$$

with the number of bodies N and power law index $q = 2.8$, consistent with shearing-box simulations of the streaming instability mechanism (Johansen et al., 2015; Simon et al., 2016, 2017). Using this power law, we generate integer radii $R_p \geq R_{p,\text{min}}$ according to

$$R_p = \lceil R_{p,\text{min}}(1 - x_{\text{rand}})^{-1/(q-1)} \rceil, \quad (15)$$

with the minimum planetesimal radius in our parameter space $R_{p,\text{min}} = 10$ km and pseudo-random number $x_{\text{rand}} = 0-1$. Depending on the regime chosen ($R_{p,\text{max}} = 20, 30, 50, 100$ km) we accept or reject radii exceeding the upper limit value, resulting in an approximate power law distribution.

Following the approach of Wetherill and Stewart (1993) (as described in Morbidelli et al., 2009, Supplementary Material therein), we build a normalized collision probability distribution of pair-encounters for the generated planetesimals during a time step δt using

$$\hat{N}_{c,ij} = N_i N_j F_{g,ij} (R_i + R_j)^2, \quad (16)$$

with bodies of different sizes i and j with their respective numbers N_i and N_j and radii R_i and R_j and gravitational focusing factor $F_{g,ij} \approx 1$ for the velocity dispersions chosen here. Next, we sample the collision probability distribution using a linear alias method to return $N_{p,\text{tot}}/2$ collision pairs ij , where $N_{p,\text{tot}}$ is the total number of bodies in the generated planetesimal family.

Each planetesimal in each collision pair is randomly assigned a formation time $t_{\text{form}} = [t_{\text{min}}, t_{\text{max}}]$, with $t_{\text{min}} = 0.1$ or 0.5 Myr, and $t_{\text{max}} = 1.5$ Myr. Additionally, we investigated a parameter space where t_{min} and t_{max} varied with collision time $t_{\text{collision}}$, such that $t_{\text{min}} = t_{\text{collision}} - \Delta t$, where $\Delta t = 0.5$ or 0.7 Myr (but $t_{\text{min}} = 0.1$ Myr at minimum and $t_{\text{min}} = 1.0/0.8$ Myr at

maximum) and $t_{\max} = 1.5$ Myr. Naturally, the maximum formation time was limited to $t_{\text{collision}}$ in case $t_{\text{collision}} < t_{\text{form,max}} = 1.5$ Myr. The collision pair is assigned a randomized impact angle $\theta = [35, 55]^\circ$ and a collision velocity $\Delta v = 0.5, 1.0, 1.5$ or 2.0 km/s, according to the specific setting. The different parameter choices are summarized in Table 2.

Table 2: Parameters for the Monte Carlo collision model with the maximum radius of a planetesimal family $R_{\text{p,max}}$, the earliest formation $t_{\text{form,min}}$, the latest formation $t_{\text{form,max}}$, the maximum planetesimal dwell time Δt and the velocity dispersion Δv . See text for details on the assumptions.

Parameter	Unit	Values
$R_{\text{p,max}}$	km	20, 30, 50, 100
$t_{\text{form,min}}$	Myr	0.1, 0.5
$t_{\text{form,max}}$	Myr	1.5
Δt	Myr	0.5, 0.7
Δv	km/s	0.5, 1.0, 1.5, 2.0

We evaluate each collision, depending on the sizes (and therefore masses, assuming constant initial densities of $\rho = 3500$ kg/m³) R_i and R_j , angle θ and impact speed Δv , employing the EDACM model of Leinhardt and Stewart (2012). If the outcome is super-catastrophic, defined as the mass of the largest intact remnant block after the collision being less than 0.1 of the combined mass, we calculate the thermal effect on the remnant material as described further below. We note that the model of Leinhardt and Stewart (2012) has recently been challenged regarding the catastrophic disruption threshold. Movshovitz et al. (2016) argue for a lower threshold value than Leinhardt and Stewart (2012), thus our estimate for super-catastrophic break-up using the EDACM scaling can be seen as a conservative approach so that we do not overestimate the number of super-catastrophic collisions, and thus potential chondrule material.

For categorizing the collisional debris, we evaluate the thermal state and material properties of each planetesimal in a collision pair before the impact using a two-dimensional bilinear interpolation from the initial $R_{\text{p}}-t_{\text{form}}$ parameter grid (see Figure 2 and Section 3.1) of the time-dependent numerical models described in Section 2.2. The injected energy from body i to j , $\Delta E_{ij} = E_{\text{kin},i} - E_{\text{pot},j}$, with the kinetic energy of impactor i , $E_{\text{kin},i}$, and potential energy of target j , $E_{\text{pot},j}$, is homogenized over the target volume via $\Delta E_{j,k} = (E_{\text{kin},i}/E_{\text{pot},j})\Delta E_{ij}$, where the target volume is subdivided into n shells with energy $E_{\text{pot},k}$. If the injected energy $\Delta E_{j,k}$ into a sub-volume of the target is greater than the energy needed to heat it to above the chondrule formation temperature $T_{\text{chondrule}}$, the material is categorized as post-collision liquid $\hat{V}_{\text{pc,chondrule}}$ ($T_{\text{post}} > T_{\text{chondrule}}$, Figure 9), normalized by the total debris volume of the colliding family of planetesimals. The necessary energy is given by

$$\Delta E_{\text{chondrule},k} = [(T_{\text{chondrule}} - T_k) \cdot c_p + L_{\text{Si}} \cdot (\varphi_{\text{chondrule}} - \varphi_k)] \cdot m_k, \quad (17)$$

with temperature T_k , minimal chondrule formation peak melt fraction $\varphi_{\text{chondrule}}$, latent heat of silicate melt L_{Si} , melt fraction φ_k and mass m_k of the specific sub-volume. If it does

not reach $T_{\text{chondrule}}$, it is counted as $\hat{V}_{\text{pc,residual}}$, further subdivided into partially melted ($T_{\text{chondrule}} > T_{\text{post}} > T_{\text{sol}}$, Figure 9) and unmelted material ($T_{\text{post}} < T_{\text{sol}}$, Figure 9). If the material exceeded the defined melt fraction threshold for metal loss φ_{crit} (0.4, 0.5 or 0.6) before the collision, the sub-volume is counted as $\hat{V}_{\text{pc,loss}}$ ($\varphi_{\text{pre}} > \varphi_{\text{crit}}$, Figure 9). We re-do these steps for each planetesimal of each collision pair for all timesteps starting from 0.1 Myr (or 0.5 Myr, Supplementary Figures) after CAI until 5 Myr after CAI, where for each timestep a new 'collision family' is generated. For instance, for model setting $t_{\text{form}} = [0.1, 1.5]$ Myr at time $t = 0.8$ Myr, the planetesimals in the colliding family were randomly drawn from a formation time interval $t_{\text{form}} = [0.1, 0.8]$ Myr; at time $t = 2.3$ Myr from a time interval $t_{\text{form}} = [0.1, 1.5]$ Myr. For model setting $t_{\text{form}} = [t_{\text{collision}} - 0.5, 1.5]$ Myr at time $t = 0.8$ Myr, the planetesimals in the colliding family were randomly drawn from a formation time interval $t_{\text{form}} = [0.3, 0.8]$ Myr; at time $t = 2.3$ Myr from a time interval $t_{\text{form}} = [1.0, 1.5]$ Myr.

The approach outlined above has several simplifications. First, the intrinsic collision probability for bodies in the sampled planetesimal orbit is chosen to be

$$P_{ij} = (\alpha_v v_{ij})/[4Ha(\delta a + 2ae_i)] = \text{const.}, \quad (18)$$

with the average collision velocity Δv , a constant depending on Δv ranging from $0.57 \leq \alpha_v \leq 0.855$ (Wetherill and Stewart, 1993), the symmetrical mutual scale height H , the semi-major axis and width a and δa of the annulus and the mean eccentricity of projectiles e_i , is chosen to be constant. Therefore, we do not simulate a global source system of generated planetesimals that collide randomly. Rather, we *ab initio* assume planetesimals that formed according to the power law slope described above and collide in pairs with a probability given by the mutual geometric factor. In other words, pairs of massive planetesimals are favored due to their larger geometrical cross-section, but eventually all planetesimals generated from the SFD do collide. Second, we consider only the simple cases of super-catastrophic interactions. In fact, catastrophic, hit-and-run, erosive and accretionary interactions could have an influence as well (Asphaug, 2010). However, for the low-mass regimes coupled with the chosen impact velocities shown here, super-catastrophic or catastrophic impacts are important and may create the majority of the debris. Third, the injected energy ΔE_{ij} is assumed to fully go into disruption and heating energy of the target material.

We use this model to demonstrate the qualitative imprint of the pre-collision interior evolution state of the planetesimals on the collisional debris in Section 3.2 and discuss its implications in Section 4.

3. Results

In this section we present the results of our models of the thermomechanical history of colliding bodies before the impact event (Section 3.1) and the outcome of the coupled evolution-collision scenario (Section 3.2).

3.1. Thermo-mechanical-chemical evolution before the collision event

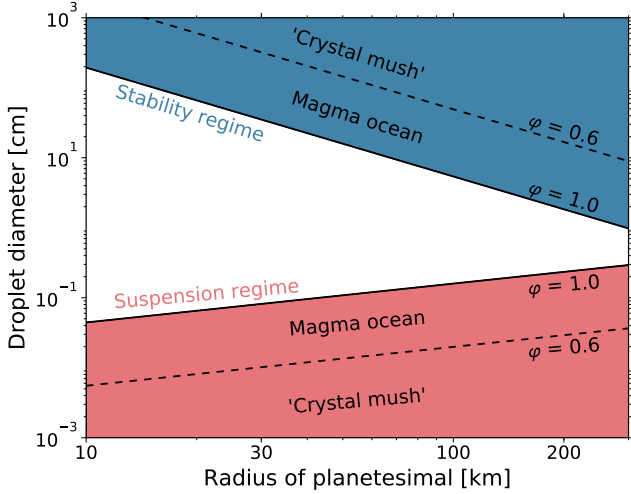


Figure 3: Droplet sizes of Fe,Ni metal versus planetesimal radius. The blue region ('stability'; Equation 9) shows the expected droplet sizes in fully-molten magma ocean planetesimals. The red region ('suspension'; Equation 7), in contrast, shows the maximum droplet sizes that can be entrained by vigorous convection for various melt fractions φ . Since the suspension limit never exceeds the stability criterion, metal droplets in fully-molten planetesimals efficiently segregate into the core. See text for details on the scalings. The considered planetesimal radius range here, and in Figure 4, corresponds to the birth-size frequency distribution suggested by Johansen et al. (2015).

Figures 3 and 4 show the results of our scaling analysis of fully-molten planetesimals. Figure 3 demonstrates that the characteristic sizes of Fe,Ni metal droplets for the expected dynamics in a planetesimal magma ocean do not allow for droplet suspension. The droplets grow to sizes larger than can be suspended by convection and will thus rapidly rain out onto the planetesimal center. Therefore, fully-molten planetesimals rapidly evolved into a physically differentiated structure.

Figure 4 shows, first, that the time scale for chemical equilibration (\sim hours to days) suggests a very fast homogenization of the material during magma ocean stages. In particular, it is much shorter than the lifetime of the protoplanetary disk ($\sim 3\text{--}5 \cdot 10^6$ yr, Alexander et al., 2014), the thermo-mechanical evolution of planetesimal interiors ($\sim 10^5\text{--}10^6$ yr, Hevey and Sanders, 2006) and the collisional evolution of an accreting planetesimal swarm ($\sim 10^4\text{--}10^5$ yr, Wetherill and Stewart, 1993). Second, the chemical equilibration time scales for the cases we consider in this manuscript lie orders of magnitudes above the characteristic collision time scales. This suggests that the primordial chemical and isotopic heterogeneities inherited from prior to accretion were homogenized rapidly after reaching the magma ocean stage. However, the equilibration time scale is not fast enough to homogenize the interior during the collision if it remained below the rheological transition before the event, since the diffusion time scale is longer than the collision time scale by orders of magnitude.

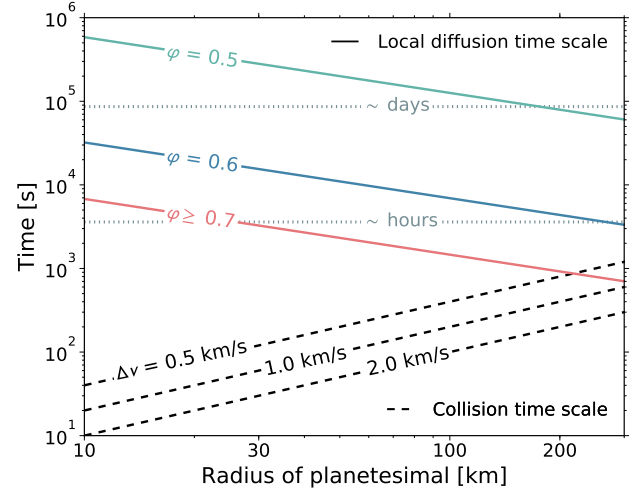


Figure 4: Radius of planetesimal versus time for either chemical equilibration (solid lines) or a planetesimal collision event (dashed lines). The solid lines ('local diffusion time scale', Equation 10) show the time scale for microscale chemical equilibration in a fully-molten magma ocean planetesimal for various silicate melt fractions φ . These are on the order of hours to days and thus demonstrate that fully-molten planetesimals rapidly chemically equilibrate. Therefore, any collisional debris from them would feature chemical signatures *unlike* chondrite material. The dashed lines ('collision time scale', Equation 12), in contrast, quantify the time it takes for an average collision of two similar-sized planetesimals to take place at various encounter velocities Δv . Up to several hundreds of km in radius, the diffusion (solid) and the collision (dashed) time scales differ by orders of magnitude. That means, if the planetesimal material was chemically unequilibrated (= *not fully-molten*) before a hypothetical impact splash event, the expanding magma plume could retain a chemically and isotopically heterogeneous signature – consistent with chondritic materials.

Figures 5 and 6 show the time-dependent thermal structure of planetesimals due to their interior evolution from ^{26}Al heating. Figure 5 shows the thermal evolution of one single model with internal melt fractions and in comparison the amount of melt produced within bodies of different sizes and formation times normalized to their total volume. In general, earlier formed and bigger planetesimals exhibited larger heating to cooling ratios, because the radiogenic heat source ^{26}Al decayed with $t_{1/2} = 0.72$ Myr, and the surface-to-volume ratios shrank drastically with increasing size of the body. This means that the thermal evolution of the low-mass planetesimals was intrinsically time- and size-dependent. Importantly, a transient regime of silicate material with temperatures around the solidus ($T_{\text{sol}} = 1416$ K) within planetesimals existed, which varied drastically with time and depth inside the bodies depending on the planetesimal sizes and formation times. Furthermore, low-mass bodies with radii $R_p \sim 10$ km exhibited partially molten states only during a narrow time interval $t \sim 0.5\text{--}2.5$ Myr after CAIs.

Figure 6 shows the maximum fractional volumes of planetesimal models that exceeded the critical melt fraction φ_{crit} . These planetesimal sub-volumes likely underwent magma ocean stages accompanied by rapid metal-silicate separation and chemical equilibration, as described in Figures 3 and 4. In particular, early formed massive planetesimals above ≥ 30 km radius with $t_{\text{form}} \leq 0.9$ Myr after

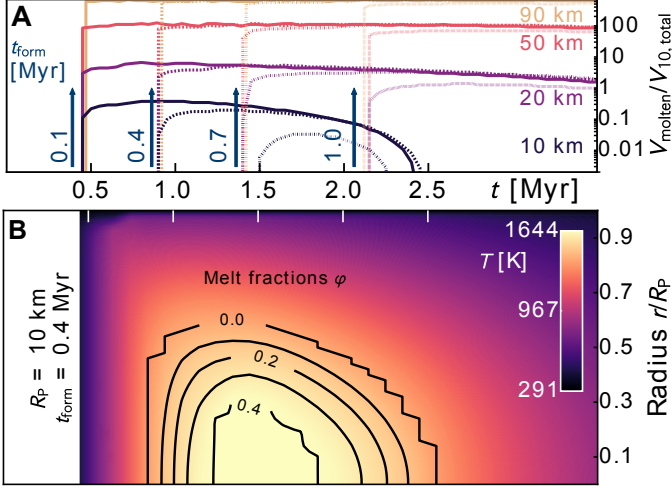


Figure 5: **(A)** Partially molten volume inside planetesimals over time, normalized by the total volume of a body with $R_p = 10$ km. The low-end mass tail of the planetesimals exhibited partially molten states only during a short time interval, e.g., from 0.5–2.5 Myr ($R_p = 10$ km). Arrows indicate formation times of associated lines. $R_p = 10$ km bodies did not exhibit any melt for $t_{\text{form}} \geq 1.2$ Myr. **(B)** Depth-dependent temperature structure for a planetesimal with $R_p = 10$ km and $t_{\text{form}} = 0.4$ Myr. Partial melt fractions (isolines) were sustained for a time period of $\Delta t \sim 1.7$ Myr after the initial heat-up phase.

CAIs were intensely heated and major parts of their total volume experienced pervasive melting periods. There is, however, a large transition regime with planetesimals mostly experiencing partial melting throughout their interiors (the transition band from black to bright yellow in Figure 6). Planetesimals that formed later than ~ 1.0 Myr, or alternatively formed with $(^{26}\text{Al}/^{27}\text{Al})_{\text{form}} \leq 1.8 \cdot 10^{-5}$, experienced only minimal melting episodes within the innermost parts of their interior.

As a transition to the coupled evolution-collision scenario in Section 3.2, Figure 7 parameterizes the required impact energy for a collision in the super-catastrophic limit. In an idealized scenario, the injected energy must be sufficient to, first heat at least parts of the target body to the required temperatures and, second, disrupt most of the target body into small pieces. In this idealized view, the most energetically favorable source of material for producing chondrules was the center of the target body, as it was hottest due to pre-heating from ^{26}Al .

Together with the melt fraction threshold for metal rain-out (φ_{crit}), this constrains the minimum required impact energy from a two-body encounter to produce chondrules in the collision (Figure 7). To give a simple example, under the assumption of perfect disruption and energy transfer between impactor and target, the minimal velocity necessary to achieve the critical chondrule formation temperature in the center of the target body is

$$\Delta v \geq \sqrt{\frac{2M_{\text{tot}}}{m_{\text{imp}}} \cdot \left(\Delta\varphi L_{\text{Si}} + \Delta T c_p - \frac{3GM_{\text{tot}}}{5R_{\text{tot}}} \right)},$$

with impactor mass m_{imp} , deviations from the required chondrule melt fraction $\varphi_{\text{chondrule}} \sim 0.86$ and temperature $T_{\text{chondrule}} = 1900$ K, $\Delta\varphi = \varphi_{\text{chondrule}} - \varphi$ and $\Delta T = T_{\text{chondrule}} - T_{\text{center}}$,

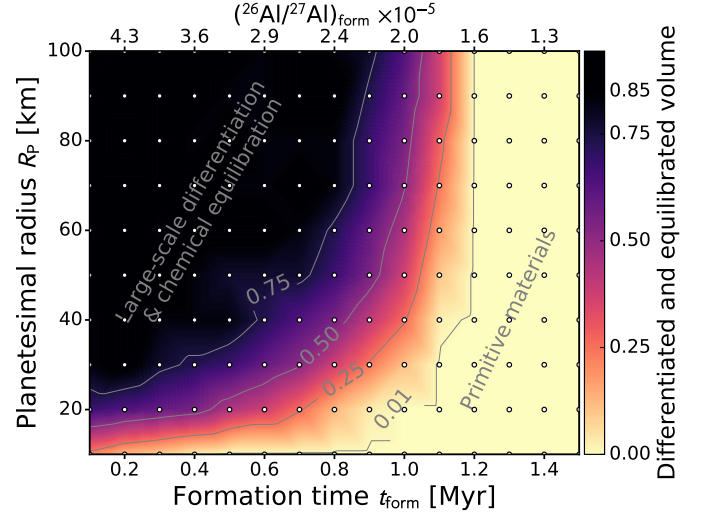


Figure 6: Volume of planetesimals which exceeded melt fractions of $\varphi \geq 0.4$ during the time interval $t = 0.1$ –5 Myr after CAIs, normalized by the total volume of each body. The value at each dot represents the maximum volume fraction throughout a single numerical simulation with the indicated R_p - t_{form} combination. Especially planetesimals with $R_p > 30$ km and $t_{\text{form}} \leq 0.9$ Myr after CAIs underwent large scale magma ocean periods and are therefore not eligible as chondrule precursor bodies. For reference, the $(^{26}\text{Al}/^{27}\text{Al})_{\text{form}}$ ratio incorporated into a body at its formation time, for a disk-wide homogeneous ^{26}Al distribution, is shown at the top.

latent heat of silicate melting $L_{\text{Si}} = 400$ kJ/kg, pre-collisional material temperature at the target center T_{center} , silicate heat capacity $c_p = 1000$ J/(kg K), Newton’s constant G , combined target-impactor mass M_{tot} and combined target-impactor radius R_{tot} . As an example, for the case of a super-catastrophic collision of two equally sized planetesimals with $R_p = 10$ km and internal silicate temperature of $T_{\text{center}} = 1600$ K, which translates to $\varphi = 1 - (T_{\text{center}} - T_{\text{sol}})/(T_{\text{liq}} - T_{\text{sol}}) \sim 0.33$, it would have required impact speeds of $\Delta v \sim 1.5$ km/s to produce post-impact material with $T_{\text{post}} \geq T_{\text{chondrule}}$. With one of the two objects being more massive, the injected energy would have increased and thus lower impact speeds would have been sufficient to produce chondrule melt sprays. Still, this calculation and the required energies from Figure 7 define approximate estimates for the impact velocities required in our analytical expression in order to form chondrules from disruptive impacts. This yields roughly $\Delta v \sim 1$ km/s and is thus presumably higher than the mutual velocities expected to arise from self-stirring of a small planetesimal swarm with radii of up to several tens of kilometers.

3.2. Collisional processing

To explore the effects of varying impact speeds on the planetesimal population, we developed a Monte Carlo approach to model the time-dependent influence of increased internal energies in the parent bodies on potential chondrule material in the collision aftermath (Section 2.3). The results from several simulation runs for planetesimal swarms with $R_p = 10$ –20 km are shown in Figure 8. In general, higher collision velocities increase the output of melt from the collision.

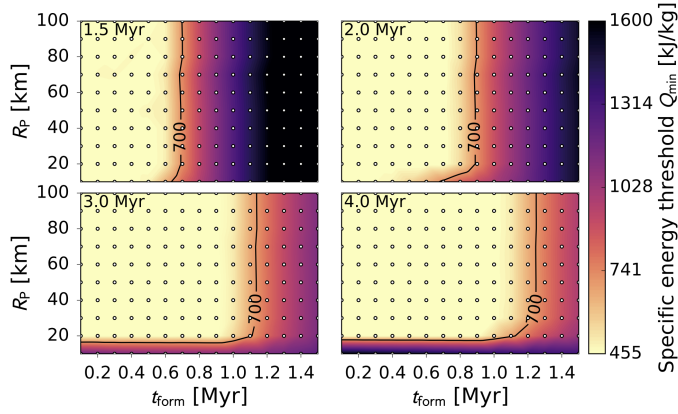


Figure 7: Evolution of the specific energy required at a given time t to raise the temperature in parts of the collisional debris to above the chondrule formation temperature: $T_{\text{post}} \geq T_{\text{chondrule}} = 1900$ K. For this calculation, we assumed homogeneous energy injection across the entire target body. Importantly, the smallest bodies were sufficiently heated during the time interval $t \sim 1.5\text{--}3$ Myr to require impact energies of $Q_{\text{min}} \sim 450$ kJ per unit mass, after which they cooled down. The evolution of the 700 kJ/kg iso-contour shows that until ~ 2 Myr after CAIs small bodies required energies below this value, after 3 Myr after CAIs they required much higher energies to form chondrules.

For several cases (like in Figure 8A), the thermal evolution from ^{26}Al heating produced a peak in eligible chondrule material output for constant collision velocities at around $t \sim 2$ Myr. If planetesimals were allowed to form during the whole interval from $t_{\text{form}} = 0.1\text{--}1.5$ Myr (Figure 8A), the output of metal-free material became noticeable after $t \geq 0.7$ Myr. If the colliding families were preferentially formed at later time intervals, metal-free output became insignificant or virtually non-existent (Figure 8B,C and Supplementary Figures). For bigger planetesimal regimes with radii up to 30, 50 or 100 km (Supplementary Figures) this trend holds, while the output of chondrule forming material relative to material output with $T_{\text{post}} < 1900$ K decreased.

It is important to note that the collisional debris showed a broad thermal distribution. Material from the inner parts of the body was heated to higher temperatures and thus higher melt fractions, whereas the outer parts of the colliding bodies may have remained cool and resulted in unmelted debris, which is not seen in chondritic meteorites. To address this issue, we have quantified the post-collisional thermal distribution for several parameter combinations and thus different collision families in Figure 9 (more in Supplementary Figures). In order to ‘suppress’ the generation of a vast amount of differentiated material (which yields basaltic droplets unlike the chondrules observed in the meteoritic record, Asphaug, 2017) the make-up and dynamics of the colliding planetesimal swarm must be either (i) primarily composed of low-mass planetesimals, (ii) formed late, or (iii) feature a low dwell time before collisional recycling. The latter would correspond to a high encounter probability, which cools the material via total disruption, fragmentation or partial break-up (Ciesla et al., 2013).

The thermal distribution, and thus the ratios of melted, par-

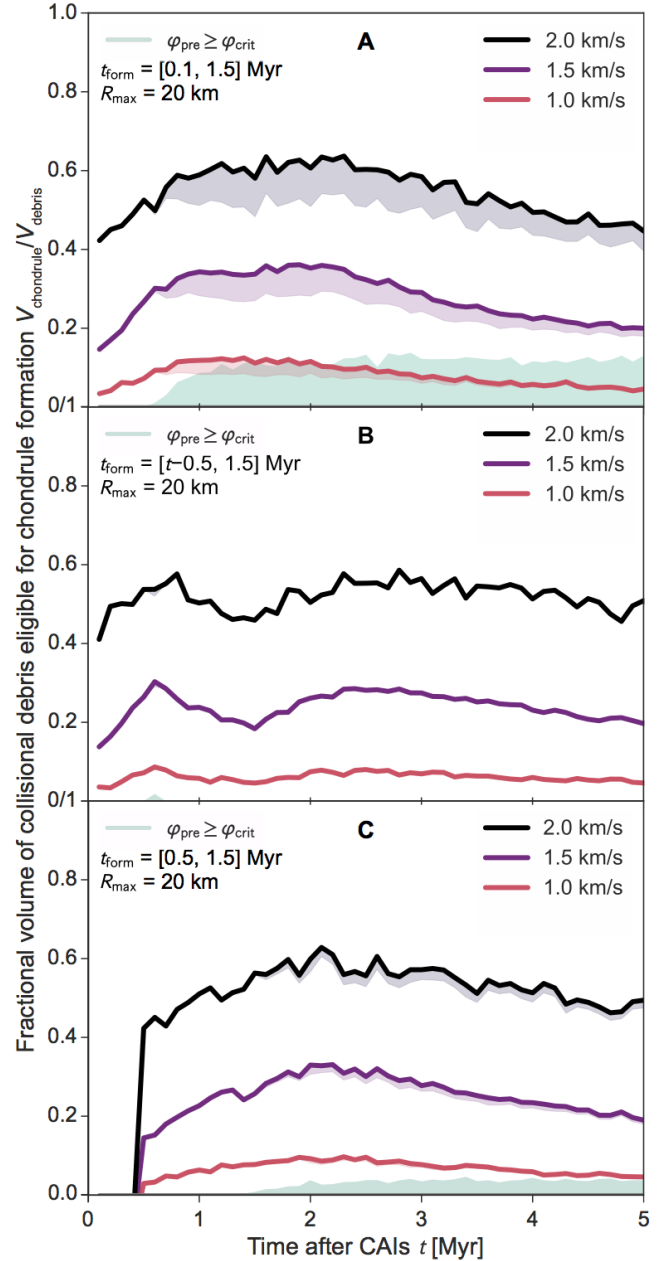


Figure 8: Output of chondrule-eligible collisional debris ($V_{\text{chondrule}}$) with post-collision temperatures $T_{\text{post}} \geq T_{\text{chondrule}} = 1900$ K over time from randomized super-catastrophic collisions, normalized to the total volume of generated debris (V_{debris}). Each line in each subplot corresponds to a single Monte Carlo simulation with varying parameters. Black lines are runs with impact velocities $\Delta v = 2.0$ km/s, purple lines $\Delta v = 1.5$ km/s and red lines $\Delta v = 1.0$ km/s. Shaded areas below these lines indicate the variation from using a different threshold for metal rain-out/chemical equilibration (φ_{crit}), with the lower bound $\varphi_{\text{crit}} = 0.4$ and the upper bound $\varphi_{\text{crit}} = 0.5$. Here, we consider bodies with $R_{\text{p}} = 10\text{--}20$ km and (A) $t_{\text{form}} = 0.1\text{--}1.5$ Myr, (B) t_{form} randomly drawn from the time interval $\Delta t = 0.5$ Myr before the collision time, and (C) $t_{\text{form}} = 0.5\text{--}1.5$ Myr. Green shaded areas show metal-depleted debris, that means, material originating from source regions with $\varphi \geq \varphi_{\text{crit}}$ before the collision. The amount of metal-depleted material decreased significantly if collisional processing was efficient and the average dwell time of intact planetesimals was short (B), or when planetesimal formation was suppressed during the early disk phase (C, Supplementary Figures).

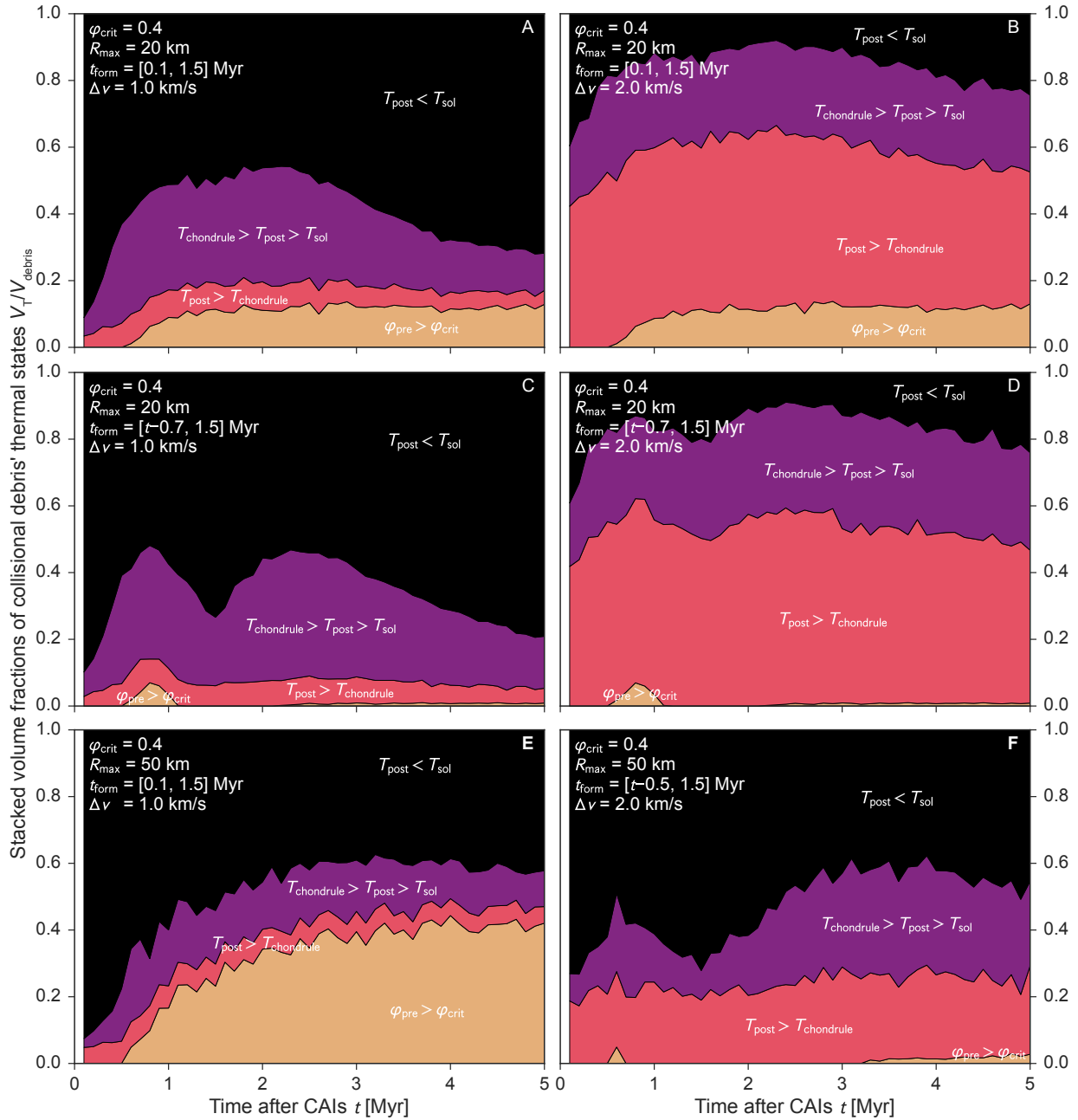


Figure 9: Thermal state of all post-collisional debris material over time for planetesimal swarms with $R_p = 10\text{--}20$ km (**A-D**) and $R_p = 10\text{--}50$ km (**E,F**), metal preservation threshold criterion $\varphi_{\text{crit}} = 0.4$ and impact velocities of $\Delta v = 1$ km/s (**A,C,E**) and $\Delta v = 2$ km/s (**B,D,F**). Each subplot corresponds to a single Monte Carlo simulation. Different colors represent post-collisional material volume with varying thermal state, normalized to the volume of the total debris generated during continuous collisional recycling. The thermal distribution of the collision aftermath depended on the specific conditions during the impact, which can change the ratio of unmelted (black, $T_{\text{post}} < T_{\text{sol}}$) to melted (purple, $T_{\text{chondrule}} > T_{\text{post}} > T_{\text{sol}}$) debris and the output of chondrules (red, $T_{\text{post}} > T_{\text{chondrule}}$). Metal-depleted material (due to metal-silicate segregation prior to collision) is depicted in yellow ($\varphi_{\text{pre}} > \varphi_{\text{crit}}$). (**B,D,F**) all show eligible-chondrule material of $V_{\text{chondrule}}/V_{\text{debris}} = 0.2\text{--}0.5\%$ throughout the time evolution. Subfigures (**C,D,F**) demonstrate the influence of a variable formation time interval in the model, representing an effective collisional grinding such that no bodies formed earlier than 0.7 Myr (**C,D**) or 0.5 Myr (**F**) before the collision time participate in the cycle. In the setting shown here, this generates some differentiated debris at ~ 0.9 Myr (**C,D,F**), but for the rest of the disk-phase prevented overheated material entering the debris cycles. (**E**) shows that larger planetesimal families readily reached debris states with a high fraction of differentiated debris (and potentially basaltic spherules as collision output). Importantly, we do not take the outcome from previous collision cycles into account, treating each time step as independent from the ones before. That implies that material labeled ‘red’ at $t = 1.0$ Myr can become ‘black’ in the next time step and vice versa for all label mutations. See Supplementary Figures for further parameter variations.

tially melted and unmelted debris, crucially depends on the localization of energy transfer during the collision. In our super-catastrophic model, however, in which the energy is

distributed across the entire body, the pre-collision temperature solely determines the temperature deviations of the post-collision debris. Depending on the formation times,

sizes and recycling efficiencies of the colliding planetesimals, the ratio of melted to unmelted debris may shift further (Supplementary Figures).

4. Discussion

4.1. Constraints from the interior evolution

The scaling analysis performed in Section 3.1 (Figures 3 and 4) demonstrates that high melt fraction regions in radiogenically heated planetesimals rapidly evolve to physically differentiated and chemically equilibrated states. We note that the scalings used in this section are based on thermal driving forces and neglect potential other effects like magnetic fields (Scheinberg et al., 2015) or rotation (King et al., 2009; Maas and Hansen, 2015) that may alter the regimes. However, any potential changes to the convection regime within magma ocean planetesimals have two effects. If turbulence is less vigorous than derived here, Fe,Ni metal settling would be even more rapid, since the energy to suspend these droplets would decrease. In the opposite case, turbulence would be more vigorous and accelerates chemical equilibration, because the diffusion time scale derived from the Kolmogorov microscales diminishes. Therefore, we conclude that any planetesimals that can serve as eligible precursor bodies for chondrule formation in a collision event cannot have been fully-molten to above the rheological transition throughout a large fraction of their interior.

In general, it is important to note that the thermal evolution – and thus degree of differentiation and chemical homogenization – forms a continuum (Figures 5, 6 and 7; compare Lichtenberg et al., 2016a). Therefore, the number of bodies that experienced substantial radiogenic preheating depends on the *local* planetesimal size frequency distribution, formation rate and recycling efficiency over time, in particular during the first 2 Myr after CAIs, during which the radiogenic heating from ^{26}Al was the predominant contributor to the internal evolution. From a thermomechanical point-of-view, the low-mass tail of planetesimals or bodies formed at sub-canonical ^{26}Al abundances (the transition region in Figure 6 and bodies labeled with ‘primitive materials’) barely incorporated enough ^{26}Al to reach temperatures near the solidus throughout most of their volume, and presumably never reached the rheological transition at melt fractions $\varphi_{\text{crit}} \approx 0.4\text{--}0.6$ (Costa et al., 2009) to develop an internal magma ocean (Lichtenberg et al., 2016a).

Regarding the Fe,Ni metal abundances in and around chondrules, it is important to note that recent laboratory experiments demonstrated the trapping of metallic liquids in planetesimal mantles with low silicate melt fractions (Bagdassarov et al., 2009; Rushmer and Petford, 2011; Holzheid, 2013; Cerantola et al., 2015; Todd et al., 2016). They showed that, first, in the regime below the silicate solidus, the high interfacial energy and wetting angle between metal-sulfide melts and solid silicate mantle minerals preclude efficient metallic core formation (Bagdassarov et al., 2009; Rushmer and Petford, 2011). Second, it was shown that in

the regime of modest silicate melt fractions, mobile basaltic melts reduce the interconnectivity and segregation of metal-sulfide liquids under deformation conditions with varying strain rates. This leaves some metallic liquid stranded in the olivine matrix until the rheological transition is reached (Holzheid, 2013; Cerantola et al., 2015; Todd et al., 2016). Above this threshold the silicate viscosity drops by orders of magnitudes and metal-silicate differentiation by gravitational settling becomes efficient (Figure 3 and Elkins-Tanton, 2012). From these experiments, we conclude that complete metal-silicate segregation in planetesimals required significant melt fractions, likely around and higher than the rheological transition. Therefore, small ($R_{\text{P}} \sim 10\text{--}30$ km) and/or late formed ($t_{\text{form}} \geq 0.7\text{--}1.0$ Myr after CAIs) planetesimals, with their presumably low melt fractions and thus incompletely differentiated interiors, can retain substantial metal abundances and chemical and isotopic heterogeneities distributed throughout most of the planetesimal volume. This qualifies these planetesimals as eligible chondrule precursor material.

Efficient collisional recycling of small or late-formed planetesimals is needed to produce large quantities of metal-bearing and chemically heterogeneous chondrules to populate the asteroid main belt with chondrite parent bodies. For that, planetesimals with modest internal melt fractions must have been abundant in the early solar system. An additional source of chondrules may have come from larger planetesimals that experienced impacts in narrow time windows during their heat-up phase, when the radiogenic preheating was sufficient but before reaching the magma ocean phase. We have qualitatively summarized the thermomechanical planetesimal regime that may be capable of chondrule formation in the aftermath of a collision in Figure 10. The regime we propose as potential chondrule precursor bodies is highlighted in green. In general, small bodies or bodies with sub-canonical ^{26}Al abundances were more likely to be heated to suitable temperatures at around their thermal maxima and to not reach melt fractions above the rheological transition throughout most of their interiors. In comparison, larger bodies featured chondrule-eligible interior states only during their initial heat-up phases.

4.2. Accretion and dynamical recycling

The results from the evolution-collision model (Section 3.2, Figures 8, 9 and Supplementary Figures) underline two points. First, planetesimals preheated by the decay of ^{26}Al require less energetic collisions than non-preheated bodies to produce chondrules in the collisional aftermath. If the bodies participating in the collision have not reached the magma ocean phase, droplets resulting from the impact can satisfy the constraints from chondrule textures, i.e., subsonic impact velocities in order to avoid shock textures in the resulting material (Asphaug, 2017). Therefore, we require velocities higher than the two-body escape speed but lower than for the case of cold planetesimals. Such velocities may be achieved during the gas disk phase (see further down). Second, Figure 9 and the additional figures for variable param-

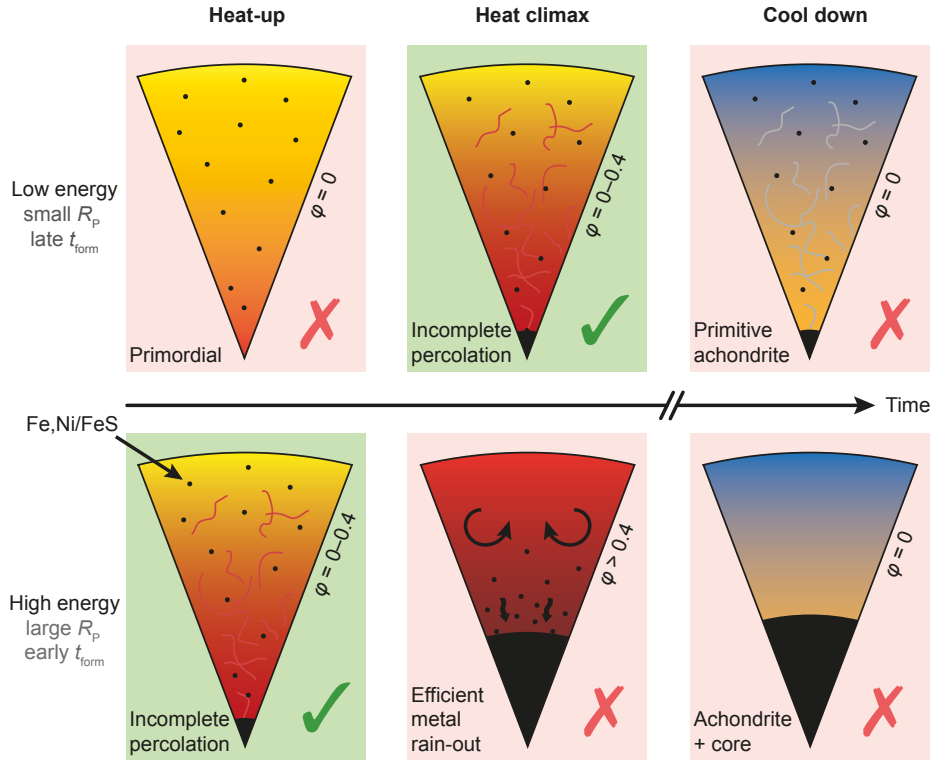


Figure 10: Schematic illustration of the qualitative thermomechanical planetesimal evolution regimes. **(Top)** Low-energy bodies with relatively small radii or late formation times, which were eligible chondrule precursor bodies (highlighted in green) around their heat climax (compare Figure 5 and Figure 7). **(Bottom)** High-energy bodies with either large radii or early formation times, which were eligible precursor bodies only during their brief initial heat-up phase. Models highlighted in red either do not feature high-enough radiogenic pre-heating (and thus would have needed implausible high impact velocities) or have lost their primordial metal abundances due to efficient metal-silicate segregation processes.

eter regimes (Supplementary Figures) demonstrate that the outcome of any collisional regime can be highly variable, depending on the local size frequency distribution (SFD), the internal state of the planetesimals and the dynamical regime of the swarm participating in the collisional processing. It underlines the necessity of simultaneously considering the *global* dynamical and *local* formation, growth and destruction mechanisms in astrophysical models of planet formation in the early solar system, which we therefore discuss here.

The first planetesimals likely formed according to a specific size frequency distribution (Johansen et al., 2007; Cuzzi et al., 2008; Chambers, 2010; Simon et al., 2016). Recent planetesimal formation models can produce bodies via the streaming instability or turbulent concentration mechanisms within the first few million years in the solar nebula (Cuzzi et al., 2008; Chambers, 2010; Carrera et al., 2015; Drażkowska et al., 2016; Schoonenberg and Ormel, 2017). Latest estimates of the initial size frequency distribution of planetesimals from the streaming instability mechanism (Johansen et al., 2015; Simon et al., 2016, 2017) converge on a power law $dN/dR_p \sim R_p^{-q}$, with the number of bodies N , the planetesimal radius R_p , index $q = 2.8$ and without an obvious lower cut-off. These estimates are consistent with the current distribution in the asteroid belt if accretional growth of small bodies via collisions and/or pebble accretion is consid-

ered (Weidenschilling, 2011; Lithwick, 2014; Johansen et al., 2015; Morishima, 2017). In such a birth-SFD, the bulk of the mass resides in massive planetesimals, while the absolute number of low-mass planetesimals exceeds the number of massive bodies by orders of magnitude. Therefore, collisions among low-mass members of the SFD outnumber interactions with one or between two massive members, even if gravitational focusing is considered. This low-mass planetesimal collision regime was most vulnerable to disruption during collisions and thus presumably created much debris from hit-and-run, erosive or (super-)catastrophic interactions (Asphaug, 2010; Leinhardt and Stewart, 2012).

The collisional dynamics and, therefore, the prevailing impact parameters crucially depend on the ambient disk conditions and the nature of planet(esimal) growth (Wetherill and Stewart, 1989, 1993; Kokubo and Ida, 1996, 1998; Weidenschilling, 2011; Johansen et al., 2015). Importantly, in a growing planetesimal swarm the parameter dominating the mean impact velocity among bodies is the size of the largest body. The largest body stirs the velocity dispersion in the swarm to its own escape velocity and the smallest bodies reach the highest relative velocities (e.g., Schlichting and Sari, 2011). During the disk stage, the velocity dispersion can be highly reduced due to gas damping, which complicates reaching sufficient impact velocities to generate chon-

drules melts. This problem originally motivated the idea of chondrule formation from fully-molten planetesimals and the sole reliance on ^{26}Al as a heat source for chondrule formation (Asphaug et al., 2011; Sanders and Scott, 2012).

Therefore, producing chondrites as N th generation planetesimals from the collisional recycling of radiogenically preheated but undifferentiated planetesimals required, first, continuous collisional reprocessing during the first few million years after the formation of the Sun. Second, sufficient velocity dispersions above the mean two-body escape velocity of the lowest-mass members of the collisional planetesimal swarm ($v_{\text{esc}} \lesssim 0.1$ km/s in the size regime evaluated here) must have been triggered. Potential stirring mechanisms to enable these enhanced mutual encounter velocities for low-mass planetesimals are manifold, for instance early formation of planetary embryos like Mars (Dauphas and Pourmand, 2011; Hasegawa et al., 2016), migration of giant planets (Walsh et al., 2011; Izidoro et al., 2016) and/or giant planets' forming cores (Raymond et al., 2016), resonant excitations (Weidenschilling et al., 1998) or implantation of planetesimals via scattering into the main belt region (Bottke et al., 2006). These mechanisms depend strongly on the ambient gas density and become more efficient as the solar nebula disperses over time, leading to decreased gas damping and allowing for higher mutual velocities.

The absolute volume of low-mass planetesimals in our solar system was presumably minor compared to the material within massive bodies (Johansen et al., 2015; Simon et al., 2016). However, it was subject to most destructive collision events among planetesimals in terms of absolute numbers. Due to their larger cross-section and enhanced gravitational focusing, the largest bodies accreted the fastest and thus presumably accumulated to form the terrestrial planets in the inner solar system (Wetherill and Stewart, 1989; Weidenschilling et al., 1997). The low-mass bodies were dynamically excited by the larger body-size population, which enhanced encounter rates. Depending on the planetesimal number and how they actually arrived at specific locations in the disk (for instance, in-situ formation versus implantation), the debris from low-mass collisions can dominate the total *local* solid density and provide the environment for the make-up of chondrite parent bodies as a result of collisionally recycled low-mass or sub-canonical- ^{26}Al planetesimals.

Recent observations and theoretical considerations estimate that the solid pile-up within 'sweet spots' in inner disk regions facilitated planetesimal formation in confined bands (Drażkowska et al., 2016; Andrews et al., 2016; Isella et al., 2016; Schoonenberg and Ormel, 2017; Carrera et al., 2017). In such narrow planetesimal birth regions with high solid density, efficient collisional processing can be enhanced because of higher collisional cross-sections and average encounter rates compared to the classical picture of disk-wide planetesimal formation. In our model, collisions of chondrule-eligible planetesimals preferentially produced a chondrule formation peak at around $t \sim 2$ Myr after CAIs (Figure 8 and Supplementary Figures). Although the exact timing depends on the parameter choice, this peak is in very

good agreement with the radiogenic ages determined for chondrules in meteorites (Villeneuve et al., 2009; Mishra and Chaussidon, 2014; Chaussidon and Liu, 2015, see chondrule geochronology Section 4.4). In our models, the peak reflects the temperature climax of planetesimals heated from ^{26}Al decay (as suggested in Sanders and Scott, 2012). Many chondrules may thus reflect collisional debris of low-mass and preheated planetesimals, whose material was not swept up by early oligarchs and survived in smaller bodies that comprise the asteroid belt today.

The asteroid belt today is significantly depleted in mass relative to the terrestrial and giant planet regions of the solar system. Therefore, either the region was dynamically depleted early-on or the mass depletion must be primordial (Bottke et al., 2006; Walsh et al., 2011; Izidoro et al., 2016; Drażkowska et al., 2016; Morbidelli and Raymond, 2016). In the latter case, this may be a suitable environment for the kind of dynamical processing we propose here and the complex transition from S- to C-type asteroids (DeMeo et al., 2015). For instance, recent studies suggest early mixing of silicate and ice-rich planetesimals (Marrocchi et al., 2016). In this picture, planetesimals may either form in lower numbers in the asteroid belt region or can be implanted from inner and outer disk regions. Thus, they would originate from distinct source reservoirs, as was suggested for iron meteorites which may have formed pre-dominantly in the inner disk region (Bottke et al., 2006).

4.3. Collision physics

In general, a complicating issue for estimates of debris generation is that the effective amount of material excavated during the collision depends on a variety of impact parameters, such as the impact velocity, impact angle, mass ratio of the colliding bodies and material compositions (Leinhardt and Stewart, 2009; Asphaug, 2010; Leinhardt and Stewart, 2012; Movshovitz et al., 2016). In addition to the amount of material ejected during the collision, it is important to understand the energy distribution in the ejected fragments/droplets. This, in turn, determines the thermal histories of chondrules produced in the collision fragments (Figures 9 and Supplementary Figures) and is crucially dependent on the energy localization during the impact, for which high-resolution three-dimensional numerical models are required. The derivation of scaling laws that account for the combined effects of ejecta size and energy distribution is a long-term goal of the impact modeling community (e.g., Ševeček et al., 2017). To our knowledge, at present there are no scaling laws that cover a large parameter space and can be used to couple the interior evolution of planetesimals prior to collision with the energy injection and material ejection during the collision.

Finally, we want to point out that, in the context of our semi-analytic evolution-collision model impacts usually require $\Delta v \gtrsim 0.5$ km/s to generate chondrule eligible material. However, using more advanced numerical collision models utilizing more realistic energy localization together with a statistical or N -body growth model (e.g., Morbidelli et al., 2009;

Schlichting and Sari, 2011; Carter et al., 2015; Johansen et al., 2015; Morishima, 2017) of the planetesimal swarm will enable much lower collision velocities. As demonstrated by Wakita et al. (2017), collisions among unheated planetesimals may already be close to generate chondrule eligible temperatures in the collision aftermath, therefore coupling both energy sources (collision and radiogenic heating) will be even more capable of producing the correct conditions.

4.4. Geochemical perspective

In this section we review some important geo- and cosmochemical constraints for the origin of chondrules and a potential collisional origin. Many interpretations of the chondrule record with respect to chondrule formation via collisions were already discussed in-depth by Sanders and Scott (2012) and partly in Connolly and Jones (2016). Even though these authors focused on fully-molten planetesimals as chondrule precursors, many of their interpretations also apply to the more moderate and realistic scenario of a radially heterogeneous interior evolution of colliding planetesimals that did not reach the magma ocean stage. Therefore, we will not repeat these arguments here, but instead focus on issues that emerged in recent years or are of direct consequence for our plead toward a more nuanced debate of collision models for chondrule formation.

Chondrule geochronology

Based on various radiometric dating techniques, chondrules formed during the first $\sim 4\text{--}6$ Myr after CAIs (Scott and Krot, 2014; Chaussidon and Liu, 2015). The exact details, however, are debated. There is an on-going debate in the cosmochemical community as to whether ^{26}Al was heterogeneously distributed in the protoplanetary disk (Larsen et al., 2011; Schiller et al., 2015; Van Kooten et al., 2016; Kleine and Wadhwa, 2017). The consequences of a heterogeneous distribution are far reaching. In the following we discuss the implications for chondrule formation by collisions of preheated planetesimals for the case of (i) a homogeneous distribution, and (ii) a heterogeneous distribution.

- (i) A homogeneous ^{26}Al distribution entails that precise Al-Mg ages of chondrules can be obtained and these indicate a time gap of $\Delta t = 0.5\text{--}1.0$ Myr between the formation of CAIs (at $t \sim 0$ Myr) and the onset of chondrule formation (Villeneuve et al., 2009; Kita and Ushikubo, 2012; Nagashima et al., 2014; Chaussidon and Liu, 2015; Villeneuve et al., 2015). In Section 4.2 we argued that the apparent peak in chondrule formation ages may be linked to the interior heat climax of ^{26}Al -heated planetesimals. However, for some parameter combinations our models do not produce a gap during the first Myr after CAI formation. The apparent time gap between CAIs and chondrules could therefore reflect protracted planetesimal formation after CAIs (Figure 6) and thus reduced ^{26}Al inventories or alternatively insufficient debris ejection from collisions during the early phase of high gas-damping. Delayed planetesimal formation may

be due to increasing dust-to-gas ratios with time due to photoevaporation (Johansen et al., 2009; Carrera et al., 2017). Decreasing ambient gas densities also allow for higher mutual velocities.

- (ii) Based on a heterogeneous distribution of ^{26}Al in our solar system, the cosmochemical record provides evidence for an extended period of chondrule formation, starting contemporaneously with CAI formation over $3\text{--}4$ Myr (Larsen et al., 2011; Connelly et al., 2012; Schiller et al., 2015; Van Kooten et al., 2016; Connelly et al., 2017). These results are inferred from Pb-Pb ages of individual chondrules. In this context, no gap needs to be reproduced, but the ^{26}Al inventory may be sub-canonical everywhere in the disk except the CAI forming region. This would shift the thermomechanical regimes in Figure 6 but would still allow for substantial radiogenic preheating depending on the local inventory of ^{26}Al at the time of planetesimal formation or reaccretion.

Nucleosynthetic, chemical and petrographic constraints

Chemical and isotopic complementarity is a concept based on elemental and isotopic studies of chondrules and matrix. Various elemental and isotope compositions may be distinct in matrix and chondrules of a specific chondrite, but, when mixed together, complement each other to nearly CI-like composition (Bland et al., 2005; Hezel and Palme, 2008, 2010; Palme et al., 2015; Ebel et al., 2016). This extends to W and Mo isotope variations derived from presolar carriers, which may also be complementary in ‘matrix’ (defined as fine-grained dust between chondrules) and chondrules (Becker et al., 2015; Budde et al., 2016a,b). These relations are often claimed to rule out particular chondrule formation mechanisms, such as a collisional origin of chondrules. Indeed, *if* complementarity of matrix and chondrules is real and indicates a genetic heritage linked by the chondrule formation process itself, this provides severe constraints on every chondrule formation mechanism suggested to date. The technical details and interpretations of the chondrule-matrix complementarity hypothesis are controversially debated in the community and out of the scope of this paper.

In recent years, it was found that terrestrial bodies in the solar system exhibit distinct nucleosynthetic isotope signatures in, e.g., Zr (Schönbächler et al., 2011; Akram et al., 2015), Ni (Regelous et al., 2008; Steele et al., 2012), Cr (Trinquier et al., 2007, 2009; Olsen et al., 2016) and Mo (Burkhardt et al., 2011). How can this be reconciled with the collisional origin of chondrules we put forward in this manuscript? In any accretion scenario the most massive planetesimals and embryos preferentially served as the early precursors of the planets. Therefore, the most massive bodies were unavailable as meteorite parent bodies because they either seeded the planet formation processes themselves or preferentially interacted with the accreting protoplanets due to gravitational focusing and enhanced geometrical encounter rates. Since accretion mechanisms like planetesimal agglomeration or pebble accretion become less ef-

ficient for smaller bodies, debris from low-mass planetesimal collisions was presumably insufficient in mass to act as a seed for planet formation. In light of chondrule formation from collisions of low-mass planetesimals, chondrites can then be interpreted as left-over material, which did not end up in planets. Instead, it either formed small parent bodies by itself or was accreted onto other relatively low-mass bodies. This implies that the materials sampled in the meteoritic record were not important contributors to the chemical bulk planet compositions in the solar system. Importantly, in this picture the chondrites sample qualitatively different material than represented in the Earth and the other terrestrial planets. This is consistent with nucleosynthetic signatures identified in meteorites, which are distinct from those of bulk Earth (Burkhardt et al., 2011; Akram et al., 2015; Palme and Zipfel, 2016).

In our model, age differences between chondrules of single chondrites can be attributed to, for instance, the storage of chondrules in outer parts of planetesimals, later liberation during disruption of the body and mixing with newly formed chondrules in the subsequent reaccretion of a new parent body. On the other hand, if age gaps in each chondrite group are narrow (as suggested by Alexander and Ebel, 2012) chondrule variability in a parent body can be obtained by mixing of debris ejecta from several chondrule-forming collisions in one annulus. Furthermore, most material eligible for chondrule formation, i.e., collisional debris, which is heated to $T_{\text{post}} > 1900$ K (Connolly and Jones, 2016; Alexander et al., 2008; Villeneuve et al., 2015) during one of the collisional cycles, not necessarily (fully) re-melts during the reprocessing. This allows chondrules to preserve relict grains – in agreement with the chondrule record (Jones, 2012) – and generates further chondrule diversity due to variable interaction of the ejected fragments with molten material and vapor in the impact plume (Villeneuve et al., 2015). Moreover, each chondrite parent body sampled a distinct, isolated reservoir without much mixing with those of other chondrite parent bodies (Jones, 2012). In the context of our model, this is a natural consequence if each chondrite parent body sampled a distinct band defined by the pile-up sweet spots for accretion (Drążkowska et al., 2016; Schoonenberg and Ormel, 2017; Carrera et al., 2017) or implantation (Bottke et al., 2006).

In our model, the ejection of material in the aftermath of the collision resulted in disconnected droplet clouds (Dullemond et al., 2014, 2016). The collision time scale in Figure 4 (Section 3.1) is comparable to the time between the heat-up of a precursor body during the collision and the separation of single droplets in the collisional aftermath. As shown in Figure 4, this time scale is orders of magnitudes shorter than the local diffusion time scale of silicate material heated to high melt fractions, i.e., to the peak temperatures of chondrules. Therefore, the cooling droplets in the collisional aftermath preserved heterogeneous primordial nucleosynthetic signatures. Such distinct signatures are reported within chondrules of the same meteorite (Olsen et al., 2016; Bauer et al., 2016). As a further contribution, these variable

chondrule signatures can also originate from different impact events, which were then mixed together during reaccretion in a subsequent accretion-collision cycle. Repeated thermal recycling of chondrules is also in line with recent studies of microchondrule formation (Bigolski et al., 2016).

In summary, we would like to emphasize that our results regarding the metal-silicate separation, chemical equilibration and the generation of variations among chondrules generally apply to both type I (FeO-poor) and type II (FeO-rich) chondrules. The presence of Fe,Ni metal varies between different chondrite groups (Davidson et al., 2014; Schrader et al., 2015) and the total amount of Fe,Ni metal within and in the vicinity of chondrules may be related to the oxygen and sulfur fugacity of the precursor body and the surrounding gaseous medium. Importantly, *any* Fe,Ni, FeS or chemical and isotopic heterogeneity present in precursor bodies before the chondrule-forming impact event would have been erased in planetesimals that experienced a magma ocean stage. As we have shown, however, it was possible to preserve these anomalies in (at maximum) partially molten precursor bodies that accreted from diverse nebular material.

4.5. Further constraints and outlook

Throughout this work we focused on geochemical and physical conditions for planetary materials *necessary* to retain abundant Fe,Ni metals, primordial isotopic and nucleosynthetic heterogeneities on a chondrule-size scale and to achieve the required peak temperatures for chondrule formation during planetesimal collisions. Further detailed work – both from modelers and experimentalists – is needed to investigate the enigmatic nature of chondrules and its link to the environment in the early solar nebula. For instance, under which circumstances can the post-collision droplet clouds satisfy the thermal histories and moderately volatile element retention (e.g., Na and K) of chondrules (Alexander et al., 2008; Dullemond et al., 2014, 2016), in case the thermal histories derived so far are reliable (Libourel and Portail, 2017)? Other important issues relate to, e.g., the prevalence of porphyritic textures among chondrules, varying chondrule distributions among different chondrite groups or the retention of relict grains. So far, there are only a few examples of chondrules which show strong experimental evidence for being generated by an impact (Krot et al., 2005; Marrocchi et al., 2016). More detailed work on the thermo-physical conditions during and after planetesimal impacts needs to be undertaken to compare theoretical expectations with experimental evidence with the goal of a *sufficient* set of evidence to either strengthen or rule out impacts as a formation mechanism for the majority of chondrules.

5. Conclusions

In this manuscript we examined the formation of chondrules from collisions of planetesimals, which were preheated from the radioactive decay of ^{26}Al . First, we investigated the end-member scenario of collisions between plan-

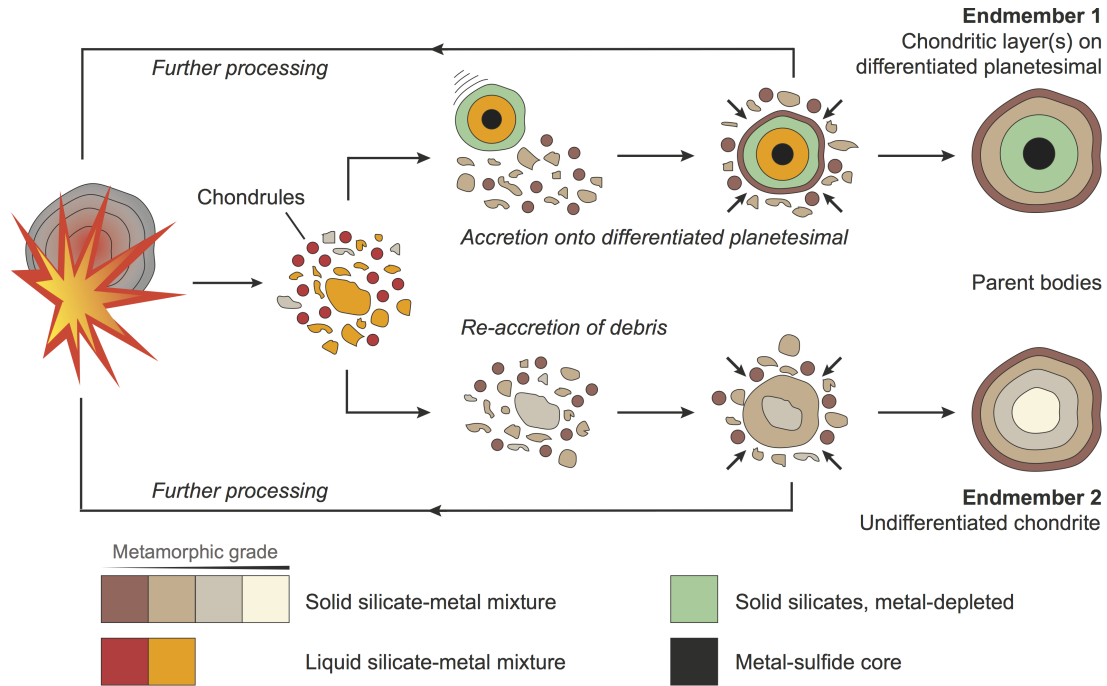


Figure 11: Schematic illustration of the accretion-collision cycles during which chondrules may form from impact splashes among radiogenically preheated planetesimals. The impacts launched expanding clouds of magma droplets (Dullemond et al., 2014, 2016) in addition to melted and unmelted debris, which subsequently cooled. The debris then either re-accumulated or accreted onto a neighboring planetesimal. Before forming the final chondrite parent bodies the material could go through multiple cycles of liberation and re-accumulation with varying degrees of injected energy and accumulation time scales. Cold matrix material (not shown) from the surrounding disk environment is accreted together with chondrules into the final chondrite parent body.

planetesimals heated to silicate melt fractions above the rheological transition, i.e., with interior magma oceans. Using well-studied scaling relations of the metal rainfall mechanism and the local diffusion time scale in convective silicate systems we determined that such planetesimals

- (i) cannot suspend significant amounts of Fe,Ni metal and, therefore, evolve to a physically differentiated structure and
- (ii) rapidly equilibrated primordial chemical and nucleosynthetic heterogeneities.

Therefore, we conclude that physically plausible impact splash interactions between such bodies would have resulted in chondrule-like but basaltic spherules, which are not observed in the meteoritic record. Contrary to Asphaug (2017), we argue that this is a telltale-sign that no such interactions took place in the early solar system and that planetesimals with large-scale interior magma oceans were not abundant in the source reservoir of today's asteroid main belt. Potential reasons for this may be delayed planetesimal formation, sub-canonical ^{26}Al abundances in the planetesimal formation region, efficient heat source redistribution by migration of aluminum-rich melts to the surface (Wilson and Keil, 2017), or widespread collisional interactions of fully-molten bodies were prevented by environmental (disk conditions) or dynamical (collisional growth-related) mechanisms, for instance, efficient collisional recycling in the source reservoir of nowadays asteroid belt. Furthermore, it would imply

that iron meteorites would have been primarily formed via incomplete metal-silicate differentiation or must originate from larger bodies than currently anticipated (Lyons et al., 2017). We suggest that these conclusions can help to achieve a better understanding of the early dynamical environment during the solar protoplanetary disk phase, because it excludes the part of the parameter space that leads to widespread generation of droplet-like and basaltic material feeding the asteroid main belt.

We argue that the debate of a collisional (or 'planetary') origin of chondrules needs to take into account the complications of the combined planetesimal evolution and recycling efficiency during accretion. The early formation and reaccretion of planetesimals of low mass and/or under sub-canonical ^{26}Al abundances opens the window to a vast collisional parameter space, which may satisfy many geo- and cosmochemical constraints derived from the meteoritic record. We have sketched one such accretion-collision cycle to generate chondrules in Figure 11. In the future, the dynamical feasibility and implications of our proposed chondrule formation scenario can be explored with astrophysical models that simultaneously solve for a global planetesimal source system and achieve sufficiently high mass resolution to resolve the low-mass bodies we focused on in this work (e.g., Levison et al., 2012; Morishima, 2017).

In summary, we propose that the linkage of the initial planetesimal size-frequency distribution, formation time, interior evolution and collisional recycling may be further used to constrain the formation of chondrules and subsequently the

chondrite parent bodies. The collisional chondrule formation scenario links the chondrule origin to the formation of the terrestrial planets and the solar system architecture we observe today. Details of the model – such as the exact disk conditions necessary to create such an environment and the thermo-physical processes and energy localization during collisions – demand detailed physical and chemical models on many spatial and temporal scales, which offer exciting new pathways for the study of planet formation. These models need to be further synchronized and tested against precise laboratory data and may ultimately lead the way to a better understanding of the earliest environment of the solar nebula.

Acknowledgements. T.L. gratefully acknowledges insightful discussions with H. Palme, J. Zipfel, N. P. Walte, J. Drążkowska, S. N. Raymond and artistic advice from A. Rozel and C. Jain. The authors thank Z. M. Leinhardt and P. J. Carter for providing us a `Python`-based script to evaluate planetesimal interactions on the basis of the `EDACM` scaling relations (Leinhardt and Stewart, 2012), C. M. O’D. Alexander and S. J. Desch for thorough and constructive reviews that considerably helped to improve the manuscript, A. Morbidelli for the editorial handling, and the organisers of the 2015 Gordon Research Conference ‘Origins of Solar Systems’ for an inspiring and collaborative meeting that initiated this project. The models were analyzed using the open source software environment `MATPLOTLIB` (Hunter, 2007). T.L. was supported by ETH Research Grant ETH-17 13-1. The numerical simulations in this work were performed on the `EULER` computing cluster of ETH Zürich. Parts of this work have been carried out within the framework of the National Center for Competence in Research PlanetS supported by the Swiss National Science Foundation.

References

- Akram, W., Schönbächler, M., Bisterzo, S., Gallino, R., 2015. Zirconium isotope evidence for the heterogeneous distribution of s-process materials in the solar system. *Geochim. Cosmochim. Acta* 165, 484–500.
- Alexander, C. M. O., Ebel, D. S., Jul. 2012. Questions, questions: Can the contradictions between the petrologic, isotopic, thermodynamic, and astrophysical constraints on chondrule formation be resolved? *Meteoritics and Planetary Science* 47, 1157–1175.
- Alexander, C. M. O., Grossman, J. N., Ebel, D. S., Ciesla, F. J., 2008. The Formation Conditions of Chondrules and Chondrites. *Science* 320, 1617.
- Alexander, R., Pascucci, I., Andrews, S., Armitage, P., Cieza, L., 2014. The Dispersal of Protoplanetary Disks. In: Beuther, H., Klessen, R. S., Dullemond, C. P., Henning, T. (Eds.), *Protostars and Planets VI*. University of Arizona Press, pp. 475–496.
- Andrews, S. M., Wilner, D. J., Zhu, Z., Birnstiel, T., Carpenter, J. M., Pérez, L. M., Bai, X.-N., Öberg, K. I., Hughes, A. M., Isella, A., Ricci, L., 2016. Ringed Substructure and a Gap at 1 au in the Nearest Protoplanetary Disk. *Astrophys. J. Lett.* 820, L40.
- Asphaug, E., 2010. Similar-sized collisions and the diversity of planets. *Chemie der Erde / Geochemistry* 70, 199–219.
- Asphaug, E., 2017. Signatures of hit-and-run collisions. In: Elkins-Tanton, L. T., Weiss, B. P. (Eds.), *Planetesimals: Early Differentiation and Consequences for Planets*. Cambridge University Press, Cambridge, pp. 7–37.
- Asphaug, E., Jutzi, M., Movshovitz, N., 2011. Chondrule formation during planetesimal accretion. *Earth Planet. Sci. Lett.* 308, 369–379.
- Bagdassarov, N., Solferino, G., Golabek, G. J., Schmidt, M. W., 2009. Centrifuge assisted percolation of Fe-S melts in partially molten peridotite: Time constraints for planetary core formation. *Earth Planet. Sci. Lett.* 288, 84–95.
- Barshay, S. S., Lewis, J. S., 1976. Chemistry of primitive solar material. *Annu. Rev. Astron. Astrophys.* 14, 81–94.
- Bauer, K. K., Schönbächler, M., Fehr, M. A., Vennemann, T., Chaumard, N., Zanda, B., 2016. Titanium and Oxygen Isotope Compositions of Individual Chondrules from Ordinary Chondrites. *LPI Contributions* 1921, 6503.
- Becker, M., Hezel, D. C., Schulz, T., Elfers, B.-M., Münker, C., 2015. Formation timescales of CV chondrites from component specific Hf-W systematics. *Earth Planet. Sci. Lett.* 432, 472–482.
- Bigolski, J. N., Weisberg, M. K., Connolly, H. C., Ebel, D. S., 2016. Microchondrules in three unequilibrated ordinary chondrites. *Meteorit. Planet. Sci.* 51, 235–260.
- Bland, P. A., Alard, O., Benedix, G. K., Kearsley, A. T., Menzies, O. N., Watt, L. E., Rogers, N. W., 2005. Volatile fractionation in the early solar system and chondrule/matrix complementarity. *Proc. Natl. Acad. Sci.* 102, 13755–13760.
- Blander, M., Pelton, A. D., Jung, I.-H., Weber, R., Dec. 2004. Non-equilibrium concepts lead to a unified explanation of the formation of chondrules and chondrites. *Meteoritics and Planetary Science* 39, 1897–1910.
- Boehler, R., von Bagen, N., Chopelas, A., 1990. Melting, thermal expansion, and phase transitions of iron at high pressures. *J. Geophys. Res.* 95, 21731–21736.
- Boss, A. P., Durisen, R. H., 2005. Chondrule-forming Shock Fronts in the Solar Nebula: A Possible Unified Scenario for Planet and Chondrite Formation. *Astrophys. J. Lett.* 621, L137–L140.
- Bottke, W., Morbidelli, A., 2017. Using the main asteroid belt to constrain planetesimal and planet formation. In: Elkins-Tanton, L. T., Weiss, B. P. (Eds.), *Planetesimals: Early Differentiation and Consequences for Planets*. Cambridge University Press, Cambridge, pp. 38–68.
- Bottke, W. F., Nesvorný, D., Grimm, R. E., Morbidelli, A., O’Brien, D. P., 2006. Iron meteorites as remnants of planetesimals formed in the terrestrial planet region. *Nature* 439, 821–824.
- Budde, G., Burkhardt, C., Brennecka, G. A., Fischer-Gödde, M., Kruijjer, T. S., Kleine, T., 2016a. Molybdenum isotopic evidence for the origin of chondrules and a distinct genetic heritage of carbonaceous and non-carbonaceous meteorites. *Earth Planet. Sci. Lett.* 454, 293–303.
- Budde, G., Kleine, T., Kruijjer, T. S., Burkhardt, C., Metzler, K., 2016b. Tungsten isotopic constraints on the age and origin of chondrules. *Proc. Natl. Acad. Sci.* 113, 2886–2891.
- Burkhardt, C., Kleine, T., Oberli, F., Pack, A., Bourdon, B., Wieler, R., 2011. Molybdenum isotope anomalies in meteorites: Constraints on solar nebula evolution and origin of the Earth. *Earth Planet. Sci. Lett.* 312, 390–400.
- Carrera, D., Gorti, U., Johansen, A., Davies, M. B., Apr. 2017. Planetesimal Formation by the Streaming Instability in a Photoevaporating Disk. *Astrophys. J.* 839, 16.
- Carrera, D., Johansen, A., Davies, M. B., 2015. How to form planetesimals from mm-sized chondrules and chondrule aggregates. *Astron. Astrophys.* 579, A43.
- Carter, P. J., Leinhardt, Z. M., Elliott, T., Walter, M. J., Stewart, S. T., 2015. Compositional Evolution during Rocky Protoplanet Accretion. *Astrophys. J.* 813, 72.
- Cerantola, V., Walte, N. P., Rubie, D. C., 2015. Deformation of a crystalline olivine aggregate containing two immiscible liquids: Implications for early core-mantle differentiation. *Earth Planet. Sci. Lett.* 417, 67–77.
- Chambers, J. E., 2010. Planetesimal formation by turbulent concentration. *Icarus* 208, 505–517.
- Chaussidon, M., Liu, M.-C., 2015. Timing of Nebula Processes That Shaped the Precursors of the Terrestrial Planets. In: Badro, J., Walter, M. (Eds.), *The Early Earth: Accretion and Differentiation*. John Wiley & Sons, Inc., Hoboken, New Jersey, pp. 1–26.
- Ciesla, F. J., Davison, T. M., Collins, G. S., O’Brien, D. P., 2013. Thermal consequences of impacts in the early solar system. *Meteorit. Planet. Sci.* 48, 2559–2576.

- Connelly, J. N., Bizzarro, M., Krot, A. N., Nordlund, Å., Wielandt, D., Ivanova, M. A., 2012. The Absolute Chronology and Thermal Processing of Solids in the Solar Protoplanetary Disk. *Science* 338, 651.
- Connelly, J. N., Bollard, J., Bizzarro, M., 2017. Pb-Pb chronometry and the early Solar System. *Geochim. Cosmochim. Acta* 201, 345–363.
- Connolly, H. C., Jones, R. H., 2016. Chondrules: The canonical and non-canonical views. *J. Geophys. Res. Planets* 121, 1885–1899.
- Costa, A., Caricchi, L., Bagdassarov, N., 2009. A model for the rheology of particle-bearing suspensions and partially molten rocks. *Geochim. Geophys. Geosys.* 10, Q03010.
- Cramer, F., Schmeling, H., Golabek, G. J., Duretz, T., Orendt, R., Buitter, S. J. H., May, D. A., Kaus, B. J. P., Gerya, T. V., Tackley, P. J., 2012. A comparison of numerical surface topography calculations in geodynamic modelling: an evaluation of the 'sticky air' method. *Geophys. J. Int.* 189, 38–54.
- Cuzzi, J. N., Hogan, R. C., Shariff, K., 2008. Toward Planetesimals: Dense Chondrule Clumps in the Protoplanetary Nebula. *Astrophys. J.* 687, 1432–1447.
- Dauphas, N., Pourmand, A., 2011. Hf-W-Th evidence for rapid growth of Mars and its status as a planetary embryo. *Nature* 473, 489–492.
- Davidson, J., Schrader, D. L., Alexander, C. M. O., Lauretta, D. S., Busemann, H., Franchi, I. A., Greenwood, R. C., Connolly, H. C., Domanik, K. J., Verchovsky, A., 2014. Petrography, stable isotope compositions, microRaman spectroscopy, and presolar components of Roberts Massif 04133: A reduced CV3 carbonaceous chondrite. *Meteorit. Planet. Sci.* 49, 2133–2151.
- DeMeo, F. E., Alexander, C. M. O., Walsh, K. J., Chapman, C. R., Binzel, R. P., 2015. The Compositional Structure of the Asteroid Belt. In: Michel, P., DeMeo, F. E., Bottke, W. F. (Eds.), *Asteroids IV*. University of Arizona Press, pp. 13–41.
- Desch, S. J., Connolly, Jr., H. C., 2002. A model of the thermal processing of particles in solar nebula shocks: Application to the cooling rates of chondrules. *Meteorit. Planet. Sci.* 37, 183–207.
- Desch, S. J., Morris, M. A., Connolly, H. C., Boss, A. P., 2012. The importance of experiments: Constraints on chondrule formation models. *Meteorit. Planet. Sci.* 47, 1139–1156.
- Drążkowska, J., Alibert, Y., Moore, B., 2016. Close-in planetesimal formation by pile-up of drifting pebbles. *Astron. Astrophys.* 594, A105.
- Dullemond, C. P., Harsono, D., Stammler, S. M., Johansen, A., 2016. Forming Chondrules in Impact Splashes II Volatile Retention. *Astrophys. J.* 832, 91.
- Dullemond, C. P., Stammler, S. M., Johansen, A., 2014. Forming Chondrules in Impact Splashes. I. Radiative Cooling Model. *Astrophys. J.* 794, 91.
- Ebel, D. S., Brunner, C., Konrad, K., Leftwich, K., Erb, I., Lu, M., Rodriguez, H., Crapster-Pregont, E. J., Friedrich, J. M., Weisberg, M. K., 2016. Abundance, major element composition and size of components and matrix in CV, CO and Acfer 094 chondrites. *Geochim. Cosmochim. Acta* 172, 322–356.
- Elkins-Tanton, L. T., 2012. Magma Oceans in the Inner Solar System. *Annu. Rev. Earth Planet. Sci.* 40, 113–139.
- Elkins-Tanton, L. T., Weiss, B. P., Zuber, M. T., 2011. Chondrites as samples of differentiated planetesimals. *Earth Planet. Sci. Lett.* 305, 1–10.
- Gail, H.-P., Henke, S., Tieloff, M., 2015. Thermal evolution and sintering of chondritic planetesimals. II. Improved treatment of the compaction process. *Astron. Astrophys.* 576, A60.
- Gerya, T. V., Yuen, D. A., 2003. Characteristics-based marker-in-cell method with conservative finite-differences schemes for modeling geological flows with strongly variable transport properties. *Phys. Earth Planet. In.* 140, 293–318.
- Gerya, T. V., Yuen, D. A., 2007. Robust characteristics method for modelling multiphase visco-elasto-plastic thermo-mechanical problems. *Phys. Earth Planet. In.* 163, 83–105.
- Ghosh, A., McSween, H. Y., 1998. A Thermal Model for the Differentiation of Asteroid 4 Vesta, Based on Radiogenic Heating. *Icarus* 134, 187–206.
- Golabek, G. J., Bourdon, B., Gerya, T. V., 2014. Numerical models of the thermomechanical evolution of planetesimals: Application to the acapulcoite-lodranite parent body. *Meteorit. Planet. Sci.* 49, 1083–1099.
- Hasegawa, Y., Wakita, S., Matsumoto, Y., Oshino, S., 2016. Chondrule Formation via Impact Jetting Triggered by Planetary Accretion. *Astrophys. J.* 816, 8–22.
- Henke, S., Gail, H.-P., Tieloff, M., Schwarz, W. H., Kleine, T., 2012. Thermal history modelling of the H chondrite parent body. *Astron. Astrophys.* 545, A135.
- Herzberg, C., Ratteron, P., Zhang, J., 2000. New experimental observations on the anhydrous solidus for peridotite KLB-1. *Geochim. Geophys. Geosys.* 1, 1051–14.
- Hevey, P. J., Sanders, I. S., 2006. A model for planetesimal meltdown by ²⁶Al and its implications for meteorite parent bodies. *Meteorit. Planet. Sci.* 41, 95–106.
- Hewins, R. H., Zanda, B., Bendersky, C., 2012. Evaporation and recondensation of sodium in Semarkona Type II chondrules. *Geochim. Cosmochim. Acta* 78, 1–17.
- Hezel, D. C., Palme, H., 2007. The conditions of chondrule formation, Part I: Closed system. *Geochim. Cosmochim. Acta* 71, 4092–4107.
- Hezel, D. C., Palme, H., 2008. Constraints for chondrule formation from Ca-Al distribution in carbonaceous chondrites. *Earth Planet. Sci. Lett.* 265, 716–725.
- Hezel, D. C., Palme, H., 2010. The chemical relationship between chondrules and matrix and the chondrule matrix complementarity. *Earth Planet. Sci. Lett.* 294, 85–93.
- Holzheid, A., 2013. Sulphide melt distribution in partially molten silicate aggregates: implications to core formation scenarios in terrestrial planets. *Eur. J. Mineral.* 25, 267–277.
- Hunter, J. D., 2007. Matplotlib: A 2d graphics environment. *Computing In Science & Engineering* 9, 90–95.
- Isella, A., Guidi, G., Testi, L., Liu, S., Li, H., Li, S., Weaver, E., Boehler, Y., Carperter, J. M., De Gregorio-Monsalvo, I., Manara, C. F., Natta, A., Pérez, L. M., Ricci, L., Sargent, A., Tazzari, M., Turner, N., 2016. Ringed Structures of the HD 163296 Protoplanetary Disk Revealed by ALMA. *Phys. Rev. Lett.* 117, 251101.
- Izidoro, A., Raymond, S. N., Pierens, A., Morbidelli, A., Winter, O. C., Nesvorný, D., 2016. The Asteroid Belt as a Relic from a Chaotic Early Solar System. *Astrophys. J.* 833, 40–58.
- Jacobson, S. A., Walsh, K. J., 2015. Earth and Terrestrial Planet Formation. In: Badro, J., Walter, M. (Eds.), *The Early Earth: Accretion and Differentiation*. John Wiley & Sons, Inc., Hoboken, pp. 49–70.
- Johansen, A., Mac Low, M.-M., Lacerda, P., Bizzarro, M., 2015. Growth of asteroids, planetary embryos, and Kuiper belt objects by chondrule accretion. *Sci. Adv.* 1, 1500109.
- Johansen, A., Oishi, J. S., Mac Low, M.-M., Klahr, H., Henning, T., Youdin, A., 2007. Rapid planetesimal formation in turbulent circumstellar disks. *Nature* 448, 1022–1025.
- Johansen, A., Youdin, A., Mac Low, M.-M., 2009. Particle Clumping and Planetesimal Formation Depend Strongly on Metallicity. *Astrophys. J. Lett.* 704, L75–L79.
- Johnson, B. C., Minton, D. A., Melosh, H. J., Zuber, M. T., 2015. Impact jetting as the origin of chondrules. *Nature* 517, 339–341.
- Jones, R. H., 2012. Petrographic constraints on the diversity of chondrule reservoirs in the protoplanetary disk. *Meteorit. Planet. Sci.* 47, 1176–1190.
- Jones, R. H., Grossman, J. N., Rubin, A. E., 2005. Chemical, Mineralogical and Isotopic Properties of Chondrules: Clues to Their Origin. In: Krot, A. N., Scott, E. R. D., Reipurth, B. (Eds.), *Chondrites and the Protoplanetary Disk*. Vol. 341 of *Astronomical Society of the Pacific Conference Series*. p. 251.
- Jones, R. H., Schilk, A. J., 2009. Chemistry, petrology and bulk oxygen isotope compositions of chondrules from the Mokoia CV3 carbonaceous chondrite. *Geochim. Cosmochim. Acta* 73, 5854–5883.
- King, E. M., Stellmach, S., Noir, J., Hansen, U., Aurnou, J. M., 2009. Boundary layer control of rotating convection systems. *Nature* 457, 301–304.
- Kita, N. T., Ushikubo, T., 2012. Evolution of protoplanetary disk inferred from ²⁶Al chronology of individual chondrules. *Meteorit. Planet. Sci.* 47, 1108–1119.
- Kita, N. T., Yin, Q.-Z., MacPherson, G. J., Ushikubo, T., Jacobsen, B., Nagashima, K., Kurahashi, E., Krot, A. N., Jacobsen, S. B., 2013. ²⁶Al-²⁶Mg isotope systematics of the first solids in the early solar system. *Meteorit. Planet. Sci.* 48, 1383–1400.
- Kleine, T., Wadhwa, M., 2017. Chronology of planetesimal differentiation. In: Elkins-Tanton, L. T., Weiss, B. P. (Eds.), *Planetesimals: Early Differentiation and Consequences for Planets*. Cambridge University Press, Cambridge, pp. 224–245.

- Kokubo, E., Ida, S., 1996. On Runaway Growth of Planetesimals. *Icarus* 123, 180–191.
- Kokubo, E., Ida, S., 1998. Oligarchic Growth of Protoplanets. *Icarus* 131, 171–178.
- Kraichnan, R. H., 1962. Turbulent Thermal Convection at Arbitrary Prandtl Number. *Phys. Fluids* 5, 1374–1389.
- Krot, A. N., Amelin, Y., Cassen, P., Meibom, A., 2005. Young chondrules in CB chondrites from a giant impact in the early Solar System. *Nature* 436, 989–992.
- Kruijer, T. S., Touboul, M., Fischer-Gödde, M., Bermingham, K. R., Walker, R. J., Kleine, T., 2014. Protracted core formation and rapid accretion of protoplanets. *Science* 344, 1150–1154.
- Larsen, K. K., Trinquier, A., Paton, C., Schiller, M., Wielandt, D., Ivanova, M. A., Connelly, J. N., Nordlund, Å., Krot, A. N., Bizzarro, M., 2011. Evidence for Magnesium Isotope Heterogeneity in the Solar Protoplanetary Disk. *Astrophys. J. Lett.* 735, L37.
- Leinhardt, Z. M., Stewart, S. T., 2009. Full numerical simulations of catastrophic small body collisions. *Icarus* 199, 542–559.
- Leinhardt, Z. M., Stewart, S. T., 2012. Collisions between Gravity-dominated Bodies. I. Outcome Regimes and Scaling Laws. *Astrophys. J.* 745, 79.
- Levison, H. F., Duncan, M. J., Thommes, E., Oct. 2012. A Lagrangian Integrator for Planetary Accretion and Dynamics (LIPAD). *Astron. J.* 144, 119.
- Libourel, G., Portail, M., Feb. 2017. Overlooked Chondrules: A High Resolution Cathodoluminescence Survey. In: *Chondrules and the Protoplanetary Disk*. Vol. 1963 of LPI Contributions. p. 2008.
- Lichtenberg, T., Golabek, G. J., Gerya, T. V., Meyer, M. R., 2016a. The effects of short-lived radionuclides and porosity on the early thermo-mechanical evolution of planetesimals. *Icarus* 274, 350–365.
- Lichtenberg, T., Parker, R. J., Meyer, M. R., 2016b. Isotopic enrichment of forming planetary systems from supernova pollution. *Mon. Not. R. Astron. Soc.* 462, 3979–3992.
- Lichtenberg, T., Schleicher, D. R. G., 2015. Modeling gravitational instabilities in self-gravitating protoplanetary disks with adaptive mesh refinement techniques. *Astron. Astrophys.* 579, A32.
- Liebske, C., Schmickler, B., Terasaki, H., Poe, B. T., Suzuki, A., Funakoshi, K.-I., Ando, R., Rubie, D. C., 2005. Viscosity of peridotite liquid up to 13 GPa: Implications for magma ocean viscosities. *Earth Planet. Sci. Lett.* 240, 589–604.
- Lithwick, Y., 2014. After Runaway: The Trans-Hill Stage of Planetesimal Growth. *Astrophys. J.* 780, 22.
- Luu, T.-H., Young, E. D., Gounelle, M., Chaussidon, M., 2015. Short time interval for condensation of high-temperature silicates in the solar accretion disk. *Proc. Natl. Acad. Sci.* 112, 1298–1303.
- Lyons, R. J., Bowling, T. J., Ciesla, F. J., Davison, T. M., Collins, G. S., Mar. 2017. Impact Effects on Cooling Rates of Iron Meteorites. In: *Lunar and Planetary Science Conference*. Vol. 48 of Lunar and Planetary Inst. Technical Report. p. 2433.
- Maas, C., Hansen, U., 2015. Effects of Earth's rotation on the early differentiation of a terrestrial magma ocean. *J. Geophys. Res. Solid Earth* 120, 7508–7525.
- Marrocchi, Y., Chaussidon, M., Piani, L., Libourel, G., 2016. Early scattering of the solar protoplanetary disk recorded in meteoritic chondrules. *Science Advances* 2, e1601001–e1601001.
- Mishra, R. K., Chaussidon, M., 2014. Fossil records of high level of ^{60}Fe in chondrules from unequilibrated chondrites. *Earth Planet. Sci. Lett.* 398, 90–100.
- Morbidelli, A., Bottke, W. F., Nesvorný, D., Levison, H. F., 2009. Asteroids were born big. *Icarus* 204, 558–573.
- Morbidelli, A., Raymond, S. N., 2016. Challenges in planet formation. *J. Geophys. Res. Planets* 121, 1962–1980.
- Morishima, R., 2017. Onset of oligarchic growth and implication for accretion histories of dwarf planets. *Icarus* 281, 459–475.
- Morris, M. A., Desch, S. J., 2010. Thermal Histories of Chondrules in Solar Nebula Shocks. *Astrophys. J.* 722, 1474–1494.
- Morris, M. A., Weidenschilling, S. J., Desch, S. J., 2016. The effect of multiple particle sizes on cooling rates of chondrules produced in large-scale shocks in the solar nebula. *Meteorit. Planet. Sci.* 51, 870–883.
- Movshovitz, N., Nimmo, F., Korycansky, D. G., Asphaug, E., Owen, J. M., 2016. Impact disruption of gravity-dominated bodies: New simulation data and scaling. *Icarus* 275, 85–96.
- Nagahara, H., Kita, N. T., Ozawa, K., Morishita, Y., Mar. 2008. Condensation of major elements during chondrule formation and its implication to the origin of chondrules. *Geochim. Cosmochim. Acta* 72, 1442–1465.
- Nagashima, K., Krot, A., Alexander, N., Huss, G. R., 2014. ^{26}Al in chondrules from CR2 chondrites. *Geochem. J.* 48, 561–570.
- Olsen, M. B., Wielandt, D., Schiller, M., Van Kooten, E. M. M. E., Bizzarro, M., 2016. Magnesium and ^{54}Cr isotope compositions of carbonaceous chondrite chondrules—insights into early disk processes. *Geochim. Cosmochim. Acta* 191, 118–138.
- Palme, H., Hezel, D. C., Ebel, D. S., 2015. The origin of chondrules: Constraints from matrix composition and matrix-chondrule complementarity. *Earth Planet. Sci. Lett.* 411, 11–19.
- Palme, H., Spettel, B., Hezel, D., 2014. Siderophile elements in chondrules of CV chondrites. *Chemie der Erde / Geochemistry* 74, 507–516.
- Palme, H., Zipfel, J., 2016. The Earth Contains a Large Fraction of Material not Represented by Meteorites. In: *Lunar and Planetary Science Conference*. Vol. 47 of Lunar and Planetary Science Conference. p. 2252.
- Ranalli, G., 1995. *Rheology of the Earth*. Chapman and Hall, New York.
- Raymond, S. N., Izidoro, A., Bitsch, B., Jacobson, S. A., 2016. Did Jupiter's core form in the innermost parts of the Sun's protoplanetary disc? *Mon. Not. R. Astron. Soc.* 458, 2962–2972.
- Regelous, M., Elliott, T., Coath, C. D., 2008. Nickel isotope heterogeneity in the early Solar System. *Earth Planet. Sci. Lett.* 272, 330–338.
- Rubie, D. C., Melosh, H. J., Reid, J. E., Liebske, C., Richter, K., 2003. Mechanisms of metal-silicate equilibration in the terrestrial magma ocean. *Earth Planet. Sci. Lett.* 205, 239–255.
- Rubin, A. E., 2017. Multiple Indicators for Multiple Melting of Chondrules. In: *Chondrules and the Protoplanetary Disk*. Vol. 1963 of LPI Contributions. p. 2006.
- Rushmer, T., Petford, N., 2011. Microsegregation rates of liquid Fe-Ni-S metal in natural silicate-metal systems: A combined experimental and numerical study. *Geochim. Geophys. Geosys.* 12, Q03014.
- Sanders, I. S., Scott, E. R. D., 2012. The origin of chondrules and chondrites: Debris from low-velocity impacts between molten planetesimals? *Meteorit. Planet. Sci.* 47, 2170–2192.
- Scheinberg, A., Fu, R. R., Elkins-Tanton, L. T., Weiss, B. P., 2015. Asteroid Differentiation: Melting and Large-Scale Structure. pp. 533–552.
- Schiller, M., Connelly, J. N., Glad, A. C., Mikouchi, T., Bizzarro, M., 2015. Early accretion of protoplanets inferred from a reduced inner solar system ^{26}Al inventory. *Earth Planet. Sci. Lett.* 420, 45–54.
- Schlichting, H. E., Sari, R., 2011. Runaway Growth During Planet Formation: Explaining the Size Distribution of Large Kuiper Belt Objects. *Astrophys. J.* 728, 68.
- Schmelting, H., Babeyko, A. Y., Enns, A., Faccenna, C., Funicello, F., Gerya, T., Golabek, G. J., Grigull, S., Kaus, B. J. P., Morra, G., Schmalholz, S. M., van Hunen, J., 2008. A benchmark comparison of spontaneous subduction models—Towards a free surface. *Phys. Earth Planet. Int.* 171, 198–223.
- Schönbächler, M., Akram, W. M., Williams, N. H., Leya, I., 2011. Nucleosynthetic Heterogeneities of Neutron-Rich Isotopes in Calcium Aluminum-Rich Inclusions and Bulk Solar System Materials. In: *Workshop on Formation of the First Solids in the Solar System*. Vol. 1639 of LPI Contributions. p. 9085.
- Schoonenberg, D., Ormel, C. W., Jun. 2017. Planetesimal formation near the snowline: in or out? *Astron. Astrophys.* 602, A21.
- Schrader, D. L., Connolly, H. C., Lauretta, D. S., Zega, T. J., Davidson, J., Domanik, K. J., 2015. The formation and alteration of the Renazzo-like carbonaceous chondrites III: Toward understanding the genesis of ferromagnesian chondrules. *Meteorit. Planet. Sci.* 50, 15–50.
- Schubert, G., Spohn, T., Reynolds, R. T., 1986. Thermal histories, compositions and internal structures of the moons of the solar system. In: *Satellites*. University of Arizona Press, pp. 224–292.
- Scott, E. R. D., Krot, A. N., 2014. *Chondrites and Their Components*. Treatise on Geochemistry 2nd ed., 65–137.
- Siggia, E. D., 1994. High Rayleigh number convection. *Annu. Rev. Fluid Mech.* 26, 137–168.
- Simon, J. B., Armitage, P. J., Li, R., Youdin, A. N., 2016. The Mass and Size Distribution of Planetesimals Formed by the Streaming Instability. I. The Role of Self-gravity. *Astrophys. J.* 822, 55.
- Simon, J. B., Armitage, P. J., Youdin, A. N., Li, R., May 2017. Evidence for universality in the initial planetesimal mass function. *ArXiv e-prints*.

- Solomatov, V. S., 2015. Magma oceans and primordial mantle differentiation. *Treatise on Geophysics* 2nd ed., pp. 81–104.
- Stammler, S. M., Dullemond, C. P., 2014. A critical analysis of shock models for chondrule formation. *Icarus* 242, 1–10.
- Steele, R. C. J., Coath, C. D., Regelous, M., Russell, S., Elliott, T., 2012. Neutron-poor Nickel Isotope Anomalies in Meteorites. *Astrophys. J.* 758, 59.
- Stolper, E., Hager, B. H., Walker, D., Hays, J. F., 1981. Melt segregation from partially molten source regions - The importance of melt density and source region size. *J. Geophys. Res.* 86, 6261–6271.
- Suzuki, A., Ohtani, E., Kato, T., 1998. Density and thermal expansion of a peridotite melt at high pressure. *Phys. Earth Planet. Int.* 107, 53–61.
- Tarduno, J. A., Cottrell, R. D., Nimmo, F., Hopkins, J., Voronov, J., Erickson, A., Blackman, E., Scott, E. R. D., McKinley, R., 2012. Evidence for a Dynamo in the Main Group Pallasite Parent Body. *Science* 338, 939–942.
- Todd, K. A., Watson, H. C., Yu, T., Wang, Y., 2016. The effects of shear deformation on planetesimal core segregation: Results from in-situ X-ray micro-tomography. *Am. Mineral.* 101, 1996–2004.
- Trinquier, A., Birk, J.-L., Allègre, C. J., 2007. Widespread ^{54}Cr Heterogeneity in the Inner Solar System. *Astrophys. J.* 655, 1179–1185.
- Trinquier, A., Elliott, T., Ulfbeck, D., Coath, C., Krot, A. N., Bizzarro, M., 2009. Origin of Nucleosynthetic Isotope Heterogeneity in the Solar Protoplanetary Disk. *Science* 324, 374.
- Trønnes, R. G., Frost, D. J., 2002. Peridotite melting and mineral-melt partitioning of major and minor elements at 22–24.5 GPa. *Earth Planet. Sci. Lett.* 197, 117–131.
- Turcotte, D. L., Schubert, G., 2014. *Geodynamics*, 3rd ed. Cambridge University Press, p. 636.
- Ševeček, P., Brož, M., Nesvorný, D., Enke, B., Durda, D., Walsh, K., Richardson, D. C., 2017. SPH/N-Body simulations of small ($D = 10\text{km}$) asteroidal breakups and improved parametric relations for Monte-Carlo collisional models. *Icarus* 296, 239–256.
- Van Kooten, E. M. M. E., Wielandt, D., Schiller, M., Nagashima, K., Thomen, A., Larsen, K. K., Olsen, M. B., Nordlund, Å., Krot, A. N., Bizzarro, M., 2016. Isotopic evidence for primordial molecular cloud material in metal-rich carbonaceous chondrites. *Proc. Natl. Acad. Sci.* 113, 2011–2016.
- Villeneuve, J., Chaussidon, M., Libourel, G., 2009. Homogeneous Distribution of ^{26}Al in the Solar System from the Mg Isotopic Composition of Chondrules. *Science* 325, 985.
- Villeneuve, J., Libourel, G., Soulié, C., 2015. Relationships between type I and type II chondrules: Implications on chondrule formation processes. *Geochim. Cosmochim. Acta* 160, 277–305.
- Wakita, S., Matsumoto, Y., Oshino, S., Hasegawa, Y., 2017. Planetesimal Collisions as a Chondrule Forming Event. *Astrophys. J.* 834, 125.
- Walsh, K. J., Morbidelli, A., Raymond, S. N., O'Brien, D. P., Mandell, A. M., 2011. A low mass for Mars from Jupiter's early gas-driven migration. *Nature* 475, 206–209.
- Wasson, J. T., Rubin, A. E., 2010. Metal in CR chondrites. *Geochim. Cosmochim. Acta* 74, 2212–2230.
- Weidenschilling, S. J., 2011. Initial sizes of planetesimals and accretion of the asteroids. *Icarus* 214, 671–684.
- Weidenschilling, S. J., Marzari, F., Hood, L. L., 1998. The Origin of Chondrules at Jovian Resonances. *Science* 279, 681.
- Weidenschilling, S. J., Spaute, D., Davis, D. R., Marzari, F., Ohtsuki, K., 1997. Accretional Evolution of a Planetesimal Swarm. *Icarus* 128, 429–455.
- Wetherill, G. W., Stewart, G. R., 1989. Accumulation of a swarm of small planetesimals. *Icarus* 77, 330–357.
- Wetherill, G. W., Stewart, G. R., 1993. Formation of planetary embryos - Effects of fragmentation, low relative velocity, and independent variation of eccentricity and inclination. *Icarus* 106, 190.
- Wick, M. J., Jones, R. H., 2012. Formation conditions of plagioclase-bearing type I chondrules in CO chondrites: A study of natural samples and experimental analogs. *Geochim. Cosmochim. Acta* 98, 140–159.
- Wilson, L., Keil, K., 2017. Arguments for the non-existence of magma oceans in asteroids. In: Elkins-Tanton, L. T., Weiss, B. P. (Eds.), *Planetesimals: Early Differentiation and Consequences for Planets*. Cambridge Planetary Science. Cambridge University Press, pp. 159–179.
- Yomogida, K., Matsui, T., 1984. Multiple parent bodies of ordinary chondrites. *Earth Planet. Sci. Lett.* 68, 34–42.

Appendix A. Supplementary Figures

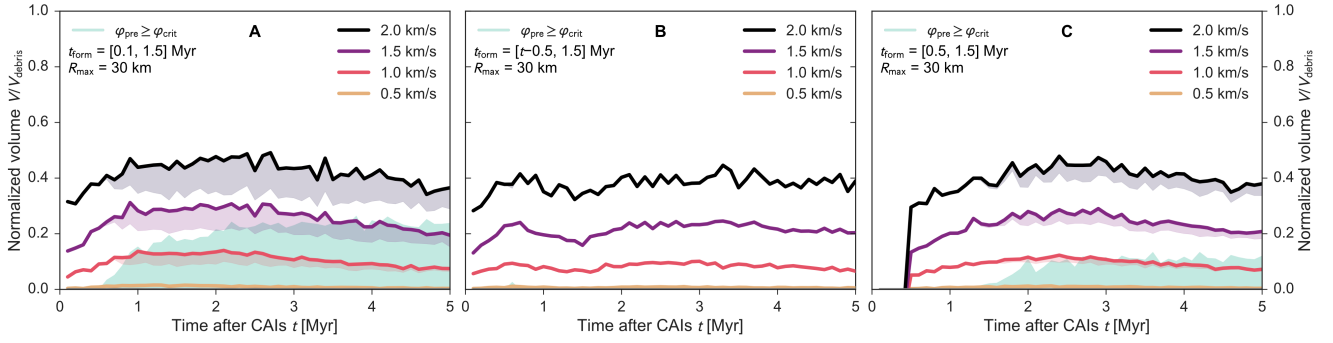


Figure A.1: Simulation outputs for planetesimal families with radii $R_{\max} = 30$ km and formation time regimes $t_{\text{form}} =$ (A) $[0.1, 1.5]$, (B) $[-0.5, 1.5]$ and (C) $[0.5, 1.5]$ Myr. See Figure 8 for a detailed description.

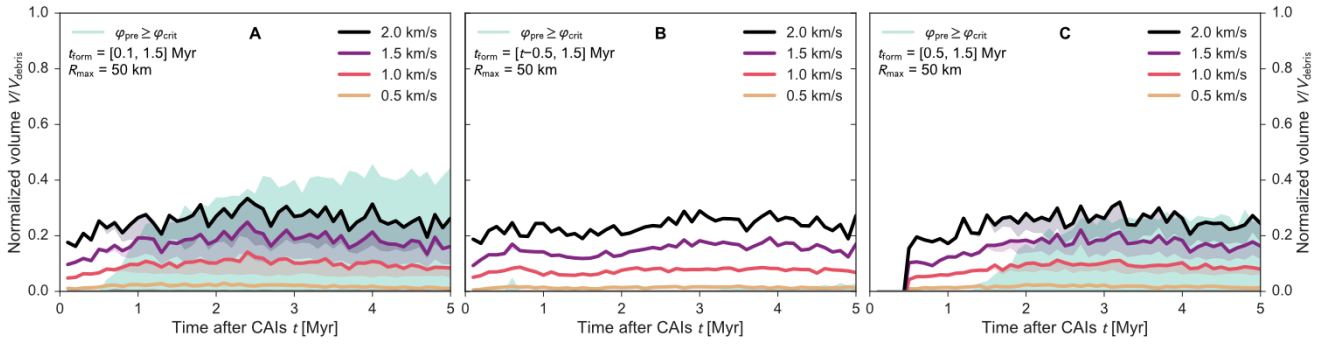


Figure A.2: Simulation outputs for planetesimal families with radii $R_{\max} = 50$ km and formation time regimes as in Figure A.1.

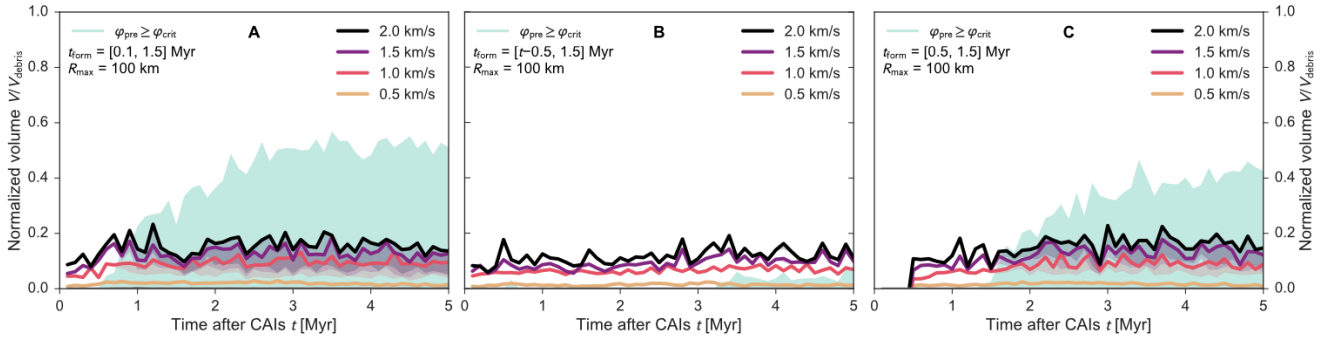


Figure A.3: Simulation outputs for planetesimal families with radii $R_{\max} = 100$ km and formation time regimes as in Figure A.1.

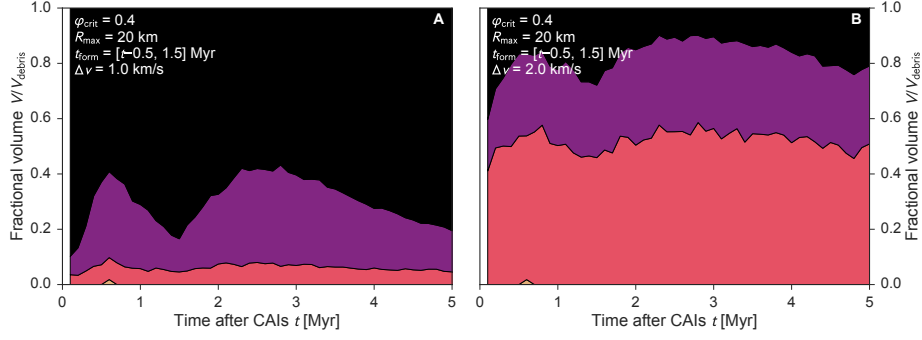


Figure A.4: Thermal debris distribution for collision models with $R_{\max} = 20$ km, $t_{\text{form}} = [-0.5, 1.5]$ Myr and collision velocities of (A) 1.0 km/s and (B) 2.0 km/s. Black represents unmelted, purple partially melted, red chondrule-eligible ($T_{\text{post}} > T_{\text{chondrule}}$) and yellow metal-depleted material. (Compare Figure 9.)

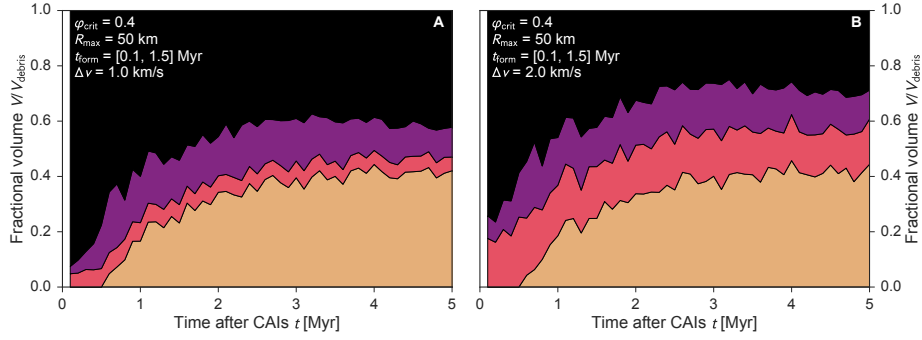


Figure A.5: Thermal debris distribution for collision models with $R_{\max} = 50$ km, $t_{\text{form}} = [0.1, 1.5]$ Myr and collision velocities of (A) 1.0 km/s and (B) 2.0 km/s. Black represents unmelted, purple partially melted, red chondrule-eligible ($T_{\text{post}} > T_{\text{chondrule}}$) and yellow metal-depleted material. (Compare Figure 9.)

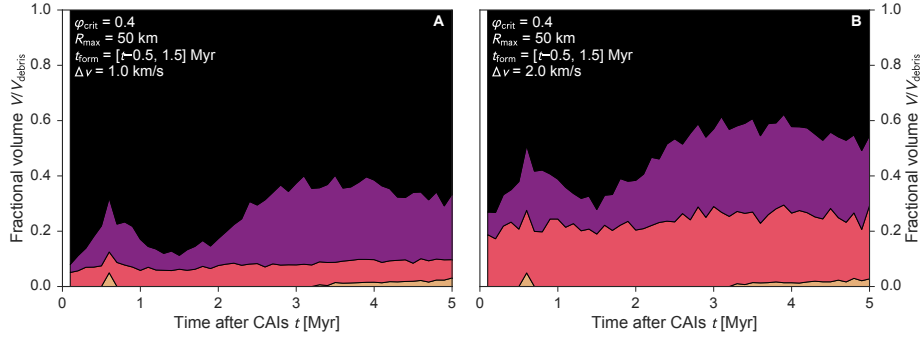


Figure A.6: Thermal debris distribution for collision models with $R_{\max} = 50$ km, $t_{\text{form}} = [-0.5, 1.5]$ Myr and collision velocities of (A) 1.0 km/s and (B) 2.0 km/s. Black represents unmelted, purple partially melted, red chondrule-eligible ($T_{\text{post}} > T_{\text{chondrule}}$) and yellow metal-depleted material. (Compare Figure 9.)

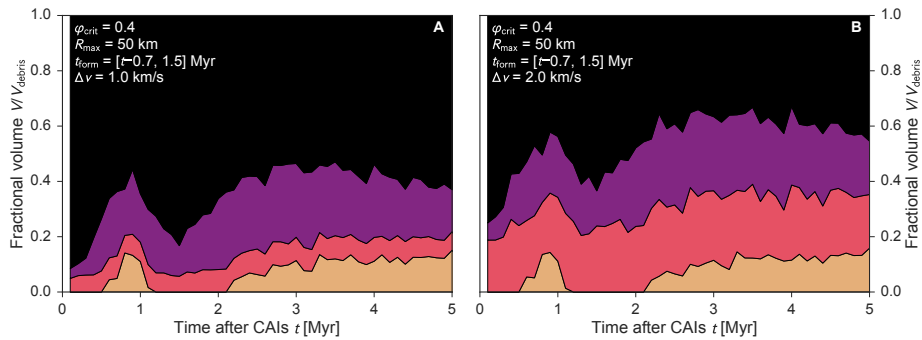


Figure A.7: Thermal debris distribution for collision models with $R_{\max} = 50$ km, $t_{\text{form}} = [-0.7, 1.5]$ Myr and collision velocities of (A) 1.0 km/s and (B) 2.0 km/s. Black represents unmelted, purple partially melted, red chondrule-eligible ($T_{\text{post}} > T_{\text{chondrule}}$) and yellow metal-depleted material. (Compare Figure 9.)

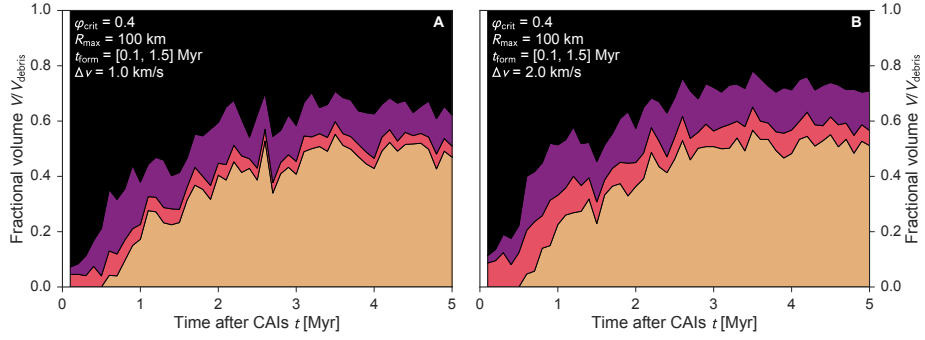


Figure A.8: Thermal debris distribution for collision models with $R_{\max} = 100$ km, $t_{\text{form}} = [0.1, 1.5]$ Myr and collision velocities of **(A)** 1.0 km/s and **(B)** 2.0 km/s. Black represents unmelted, purple partially melted, red chondrule-eligible ($T_{\text{post}} > T_{\text{chondrule}}$) and yellow metal-depleted material. (Compare Figure 9.)

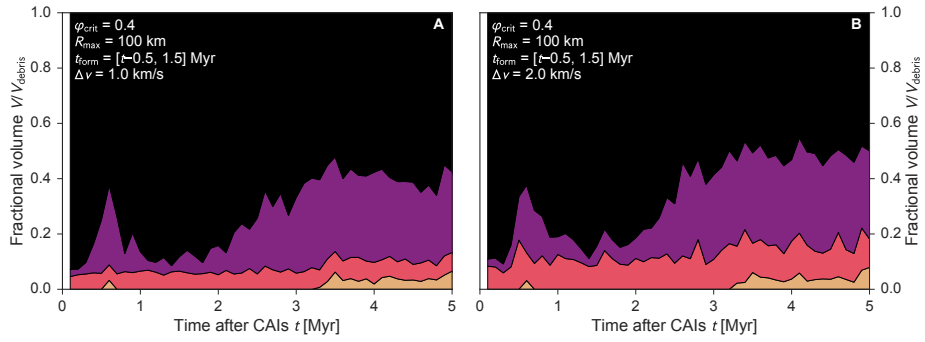


Figure A.9: Thermal debris distribution for collision models with $R_{\max} = 100$ km, $t_{\text{form}} = [t-0.5, 1.5]$ Myr and collision velocities of **(A)** 1.0 km/s and **(B)** 2.0 km/s. Black represents unmelted, purple partially melted, red chondrule-eligible ($T_{\text{post}} > T_{\text{chondrule}}$) and yellow metal-depleted material. (Compare Figure 9.)

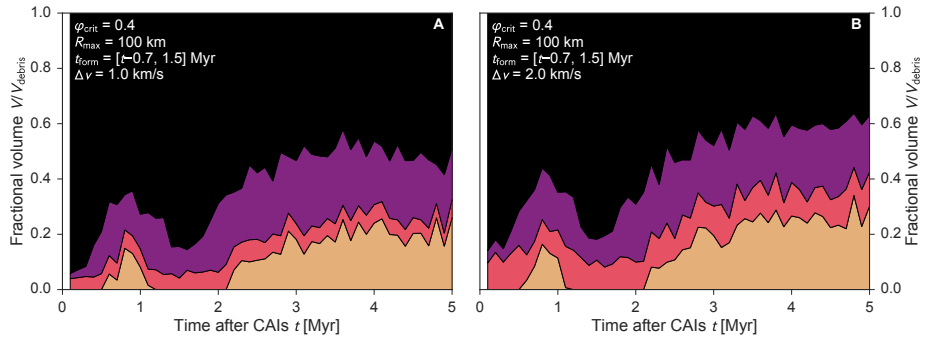


Figure A.10: Thermal debris distribution for collision models with $R_{\max} = 100$ km, $t_{\text{form}} = [t-0.7, 1.5]$ Myr and collision velocities of **(A)** 1.0 km/s and **(B)** 2.0 km/s. Black represents unmelted, purple partially melted, red chondrule-eligible ($T_{\text{post}} > T_{\text{chondrule}}$) and yellow metal-depleted material. (Compare Figure 9.)